Transcriptomics reveal a molecular signature in the progression of nonalcoholic steatohepatitis and identifies PAI-1 and MMP-9 as biomarkers in *in vivo* and *in vitro* studies

YAO ZHAO[1], MIRENSHA YAKUFU[1], CHONG MA[1], BAICAI WANG[1], JIANHUA YANG[1,2] and JUNPING HU[1]

[1]College of Pharmacy, Xinjiang Medical University, Urumqi, Xinjiang Uygur Autonomous Region 830017;
[2]Department of Pharmacy, The First Affiliated Hospital of Xinjiang Medical University, Urumqi, Xinjiang Uygur Autonomous Region 830054, P.R. China

Received June 28, 2023; Accepted October 13, 2023

DOI: 10.3892/mmr.2023.13138

Abstract. Nonalcoholic steatohepatitis (NASH) is emerging as the primary driver of liver disease-induced fibrosis. The imperative need for noninvasive biomarkers to ascertain disease progression stage is evident. The present study elucidated the biological roles of hub genes that could potentially serve as diagnostic markers for NASH. Using an *in vivo* approach, C57BL/6J mice were subjected to a high-fat and fructose diet (HFFD) for 6, 10, 14, 18 or 22 weeks. Serological biochemical indices were assessed and liver specimens were obtained to identify potential markers linked to the NASH process, employing a comprehensive strategy that combined transcriptomic and histopathological analyses. The HFFD regimen induced hyperlipidemia, obesity and insulin resistance, progressively culminating in NASH with fibrosis over time. The transcriptomic analyses indicated temporal patterns of pivotal gene sets intricately connected to NASH progression, which encompassed processes such as glucose homeostasis, inflammatory responses, reactive oxygen species-mediated damage, lipid metabolism disruptions and the formation of fibrotic tissue. Among these genes, Serpine1 and Mmp9 demonstrated promising diagnostic potential for NASH, with their intrahepatic mRNA expression levels serving as robust indicators. Moreover, the levels of PAI-1 (encoded by the Serpine1 gene) and MMP-9 in the serum of mice demonstrated a parallel increase with the duration of HFFD intervention. *In vitro* experiments utilizing HepG2 cells further validated these findings, demonstrating a significant elevation in the protein expression levels of both PAI-1 and MMP-9 upon exposure to free fatty acids, in agreement with the results of the animal study. Consequently, PAI-1 and MMP-9 are promising noninvasive biomarkers for assessing the progression of NASH.

Correspondence to: Professor Jianhua Yang, Department of Pharmacy, The First Affiliated Hospital of Xinjiang Medical University, 137 Liyushan Road, Urumqi, Xinjiang Uygur Autonomous Region 830054, P.R. China
E-mail: yjh_yfy@163.com

Professor Junping Hu, College of Pharmacy, Xinjiang Medical University, 393 Xinyi Road, Urumqi, Xinjiang Uygur Autonomous Region 830017, P.R. China
E-mail: hjp_yxy@163.com

Abbreviations: NAFLD, nonalcoholic fatty liver disease; NASH, nonalcoholic steatohepatitis; HFFD, high-fat and fructose diet; NEFA, non-esterified fatty acids; ALT, alanine aminotransferase; AST, aspartate aminotransferase; HA, hyaluronic acid; LN, laminin; PC-III, type III pre-collagen; IV-C, type IV collagen

Key words: transcriptome, biomarkers, nonalcoholic steatohepatitis, liver fibrosis, PAI-1, MMP-9

Introduction

Nonalcoholic fatty liver disease (NAFLD) is a pathological condition characterized by the excessive accumulation of fat within liver cells, unrelated to alcohol consumption or other recognized liver injury factors (1). The ailment can be categorized into four stages: i) Simple fatty liver (NAFL); ii) nonalcoholic steatohepatitis (NASH); iii) liver fibrosis; and iv) liver cirrhosis (2). The prevalence of NAFLD has experienced a sharp rise globally, reaching 25% due to the escalating number of individuals affected by obesity (3). NAFLD has evolved into a substantial public health concern due to its high prevalence, association with metabolic disorders, such as obesity, insulin resistance and dyslipidemia, and potential progression toward advanced liver disease (4). During the progression of NAFLD, 5-20% of patients initially diagnosed with simple hepatic steatosis will develop NASH (5). Serving as an inflammatory subtype of NAFLD, NASH represents a severe liver disorder characterized by hepatic steatosis, hepatocyte ballooning and lobular inflammation (6). NASH constitutes a significant transitional phase from simple hepatic steatosis to more severe liver ailments, and ~25% of patients with NASH will develop liver fibrosis (7). In the absence of proper medical intervention, NASH can culminate in liver cirrhosis and hepatocellular carcinoma (8). Recent findings have also identified its involvement as a cofactor in cardiovascular disease and other life threatening cancers, further emphasizing

its critical implications (9). Consequently, the identification of patients with NASH at an elevated risk of progressing to end stage liver disease is imperative for effective risk assessment and management (10,11). Moreover, Steatosis, Activity, and Fibrosis activity score ≥2 (sum of ballooning and inflammation) (12) or NASH activity score (NAS) ≥4 (sum of steatosis, ballooning and inflammation) (13) is considered indicative of high risk NASH, signifying an elevated probability of disease progression (14). NAFLD is a dynamic condition, with varying steatohepatic activity over time and fibrosis stages that can either progress or regress, contingent upon diverse genetic, dietary, exercise, epigenetic and environmental factors (15). The identification of efficacious biomarkers for risk stratification and approved pharmacological treatments represent major challenges in NAFLD management (16). The identification of reliable biomarkers for risk stratification is pivotal in NAFLD management, as it facilitates the prediction of disease progression and the identification of patients requiring more intensive treatment (17).

Currently, liver biopsy remains the preferred method for diagnosing NASH, utilizing pathological examination (18). However, this method has inherent limitations, including procedural complexities, high expenses, invasiveness and the potential for sampling variability, among others, which prevent its widespread adoption (19). While diagnostic models based on NASH risk factors have seen limited application, biomarkers targeting key mechanisms in NAFLD pathogenesis exhibit lower accuracy compared with histology (20). The exploration of novel, effective biomarkers is therefore warranted, requiring a deeper comprehension of the physiological mechanisms underpinning NASH. Consequently, the development of noninvasive biomarkers has become imperative to supplant invasive diagnostic procedures such as liver biopsy while accurately predicting the presence and severity of NASH (21). Predictive scores, such as the fibrosis-4 score (22) and the NAFLD fibrosis score (23), have been devised to evaluate fibrosis in NAFLD. However, their performance can vary according to the studied population, occasionally yielding indeterminate results (24). Moreover, these scores fail to provide insightful perspectives into the underlying mechanisms of NASH, which is pivotal for targeted therapeutic advancements (25). Direct fibrosis markers, including the enhanced liver fibrosis score, N-terminal type III collagen propeptide and a blood-based biomarker panel, have been utilized for the prediction of fibrosis and/or NASH susceptibility (26-28). Nevertheless, these markers possess limitations, such as reduced accuracy in identifying the presence of a condition in individuals who test positive or their exclusive applicability to high risk NASH populations without independently assessing significant fibrosis subgroups (29). Consequently, further research is imperative to develop more precise and dependable biomarkers for risk stratification in NAFLD (30-32). Additionally, these tools lack the ability to capture the dynamic nature of fibrosis progression or regression. This inherent lack of specificity and granularity has hindered the identification of prospective biomarkers for early diagnosis and therapeutic strategies for NAFLD (33). Thus, a more comprehensive and sophisticated approach is required to comprehensively grasp the dynamic nature of disease progression and identify potential intervention targets. As a result, efforts have intensified in the development of serum (plasma) biomarkers capable of assessing NASH-related hepatic fibrosis and its dynamics (34,35).

Human serum and plasma serve an indispensable role in the exploration of biomarkers and pathways, given the intricate complexity and diverse array of circulating proteins implicated in fundamental biological processes (36,37). A comprehensive understanding of the molecular anomalies underlying NAFLD progression has been attained through the analysis of liver tissue transcriptomes obtained from affected patients (17,38,39). The identification of specific proteins associated with NAFLD progression enables the development of noninvasive diagnostic tools capable of gauging NAFLD severity and predicting disease advancement. Furthermore, the discovery of serum biomarkers linked to NAFLD holds the potential to unveil novel therapeutic targets for its treatment. Authoritative studies have proposed that serum biomarkers such as fibroblast growth factor 21 and cytokeratin-18 exhibit promise as potential targets for NAFLD treatment (40-42). Moreover, the identification of novel serum biomarkers for NAFLD diagnosis and prognosis has been reported to expedite the identification of novel therapeutic targets (43-45). These findings underscore the substantial potential of serum biomarkers as targets for NAFLD treatment, meriting further research in this realm (46).

The existing comprehension of disease pathogenesis in NAFLD predominantly relies on investigations that focus on a solitary time point, typically corresponding to end stage disease (16). Nonetheless, this approach fails to provide insight into the temporal dynamics and chronological progression of the disease, aspects that remain inadequately understood (10). The objective of the present study was to delve into the progression of NASH and fibrosis in mice subjected to a high-fat and fructose diet (HFFD) via a comprehensive time-course study. Emphasis was placed on scrutinizing the temporal fluctuations in pivotal mechanisms implicated in the development of these conditions. Transcriptomic analysis of liver tissues identified an array of proteins potentially secreted into the serum of mice afflicted with NASH and/or fibrosis. In the pursuit of unraveling the molecular processes which underlie active fibrosis, a combined strategy was adopted, encompassing transcriptomics and histopathological data within the framework of integrative systems biology. To assess the clinical significance and prospective applicability of these findings, an evaluation of their translational utility was deemed necessary. The diagnostic capability was gauged using human NASH datasets and subsequently validated alterations in protein expression at the cellular level.

Materials and methods

Animal temporal study. For the present study, male C57BL/6J mice (weight, 18±2 g) at four weeks of age were housed in a pathogen-free animal facility at Xinjiang Animal Testing Center Research (Urumqi, China), where they were accommodated in group housing and provided unrestricted access to food and water. The room maintained controlled temperature conditions (20-24°C, 40-60% relative humidity) and followed a 12 h light/dark cycle. This experimental protocol

received ethical approval from The Xinjiang Animal Testing Center Research Animal Ethics Committee (Urumqi, China; approval no. XJIMM-20210417) and all research involving animals adhered strictly to globally acknowledged standards and regulations.

The mice were randomly allocated into two groups, each with distinct dietary regimens (n=6/group): i) Normal diet (chow diet from Jiangsu Xietong Biomedical Engineering Co., Ltd.) along with distilled water; and ii) High fat (HF) diet (60% HF diet from Jiangsu Xietong Biomedical Engineering Co., Ltd.) along with a 4% w/v aqueous fructose solution (Shanghai Aladdin Biochemical Co., Ltd.), both groups were assessed at 0, 6, 10, 14, 18 and 22 weeks. The chow diet consisted of 20% protein, 10% fat and 70% carbohydrate in terms of caloric content, whereas the high fat diet was comprised of 20% protein, 60% fat and 20% carbohydrate. The inclusion of 4% w/v fructose in the high fat diet equated to the high level of fructose consumption reported in adults, which amounts to 90 g/day (47).

All experimental procedures were performed during the light phase. Mice were euthanized at 6, 10, 14, 18 and 22 weeks after the initiation of the respective diets. At 4 week intervals, a subset of overnight fasted mice were euthanized by deep anesthesia with pentobarbital sodium (100 mg/kg, intraperitoneally) followed by cervical dislocation. Blood samples were obtained via the eye for serum collection. Liver tissues were isolated, with a portion fixed in 10% formalin (24 h at room temperature) and embedded in paraffin wax for conventional histochemical examination and another segment flash-frozen in liquid nitrogen and stored at ultralow temperatures (-80˚C) until analysis. This approach facilitated precise RNA isolation for subsequent transcriptomics profiling.

Biochemical analysis. Total serum triglyceride, total cholesterol, low-density lipoprotein-cholesterol, high-density lipoprotein-cholesterol and non-esterified fatty acids (NEFAs) were quantified using commercial assay kits (cat. nos. A111, A110, A113, A112 and A042; Nanjing Jiancheng Bioengineering Institute). Serum alanine aminotransferase (ALT) and aspartate aminotransferase (AST) levels were determined through spectrophotometric activity assays (cat. nos. C010 and C009; Nanjing Jiancheng Bioengineering Institute). Hepatic and serum malondialdehyde (MDA), superoxide dismutase (SOD) and glutathione peroxidase (GSH-px) were measured using a colorimetric method (cat. nos. A003, A001 and A005; Nanjing Jiancheng Bioengineering Institute). Blood glucose levels were determined immediately after sampling using a handheld glucose analyzer. Serum insulin levels were determined utilizing a mouse insulin enzyme-linked immunosorbent assay (cat. no. H203; Nanjing Jiancheng Bioengineering Institute). Insulin resistance was evaluated through the Homeostatic Model Assessment for Insulin Resistance (48), calculated as fasting plasma insulin (μg/l) multiplied by fasting plasma glucose (mmol/l) and then divided by 22.5. IL-6, IL-1β and TNF-α levels in serum were assessed using commercial assay kits employing the ELISA method (cat. nos. E20012, E20533 and E20220; Xingtai Sinobest Biotech Co., Ltd.). Serum liver fibrosis-related markers, including hyaluronic acid (HA), laminin (LN), type III precollagen (PC-III) and type IV collagen (IV-C), were analyzed utilizing commercial assay kits and the ELISA method (cat. nos. JL20576, JL20286, JL20127 and JL20170; Shanghai Jianglai Biological Technology Co., Ltd.). All kits were used according to the manufacturer's protocols.

Liver histologic analysis. Once the wax block had been properly trimmed, it was positioned on a paraffin microtome for sectioning at a thickness of 4 μm. The resultant sections were then placed in a 40˚C water bath to prevent inadvertent folding. The sections were then lifted using a glass slide and dried in a 60˚C oven. subsequently, the sections were stored at room temperature. For the histological analysis of the liver, a transverse section of the median lobe measuring 3 μm in thickness was prepared and subjected to staining with hematoxylin for 15 min and eosin for 1 min at room temperature. An impartial evaluation of NAFLD was performed by a liver pathologist, utilizing a generalized scoring system relevant to rodent models. This system was derived from the grading criteria established for the NAS (12), defined as the sum of steatosis (0-3), inflammation (0-3), and hepatocyte ballooning (0-2). To assess the degree of hepatic fibrosis, the Kleiner classification system (13), using a 5-point scale (F0-F4), was employed. The histological assessment of fibrosis necessitated the staining of tissue samples using the Masson's Trichrome Stain Kit (cat. no. G1340; Beijing Solarbio Science & Technology Co., Ltd.), according to the manufacturer's protocol. Images were captured using a light optical microscope (Leica DM2000, Leica Microsystems GmbH). ImageJ 1.8.0 (National Institutes of Health) is used for the analysis of pathological tissue sections.

Biomarker selection and identification

Transcriptomic analysis of the liver. Ambion total RNA isolation kit (cat. no. AM1912; Thermo Fisher Scientific, Inc.) was used to extract RNA from the livers of mice that were subjected to either chow or HFFD diets at multiple time points (n=3 for both groups) 6, 10, 14, 18 and 22 weeks). The quality and concentration of the RNA was determined spectrophotometrically using a Nanodrop 1000 (Thermo Fisher Scientific, Inc.). The Illumina TruSeq RNA Sample Prep kit (cat. no. RS-122-2001; Illumina, Inc.) was used for the library preparation according to the manual.

Prepared libraries were performed by VAHTS Stranded mRNA-seq Library Prep Kit (cat. no. NR612-01; Vazyme Biotech Co., Ltd.) according to the manual. Qubit 2.0 (Invitrogen; Thermo Fisher Scientific, Inc.) was used to detect the concentration of the library, and the loading concentration of the library were pooled at 10 nM concentration, we performed the 2x150 bp paired-end sequencing (PE150) and an average read depth of 15 million read pairs per library on an Illumina Novaseq™ 6000 (Illumina, Inc.) following the vendor's recommended protocol. Differentially expressed genes (DEGs) were identified at weeks 6, 10, 14, 18 and 22 utilizing the DEseq method (version 1.2.10; https://bioconductor.org/packages/release/bioc/html/DESeq2.html) (49). The statistical significance of protein-coding genes was determined by establishing a false discovery rate-corrected q-value <0.05, coupled with a fold change exceeding |1.2|. The enrichment analysis including Gene Ontology (GO; https://www.geneontology.org/) and Kyoto Encyclopedia of Genes and Genomes

(KEGG; https://www.genome.jp/kegg/) was performed with cluster Profiler R package (4.8.3; https://bioconductor.org/packages/release/bioc/html/clusterProfiler-html) (50). For the validation study, RNA-sequencing data from the GSE135251 dataset (35) were scrutinized, dataset were downloaded from the GEO database (www.ncbi.nlm.nih.gov/geo/). This dataset comprised hepatic transcriptome information from 206 patients with histologically characterized NAFLD, collected from the European NAFLD Registry. To identify genes whose hepatic expression changes were reflected peripherally, we focused on the predicted secreted proteins according to the Human Protein Atlas database (proteinatlas.org/).

Reverse transcription quantitative PCR assay. The procedure for preparing liver tissue samples is outlined as follows: i) A small quantity of liver tissue was placed into a grinding tube containing 2 ml of TRIzol® lysis solution (cat. no. 15596026; Thermo Fisher Scientific, Inc.); ii) steel grinding beads were added, and the tissue was ground at 60 Hz for 90 sec; iii) the resultant liver tissue homogenate was transferred to a 1.5 ml Eppendorf tube and 200 μl of chloroform was added; iv) the mixture was vigorously shaken for 15 sec and subsequently subjected to centrifugation at 12,000 x g for 15 min at 4˚C. Following this, total RNA was extracted from a 300 μl mixture using a nucleic acid extraction kit (cat. no. DP431; Tiangen Biotech Co., Ltd.) according to the manufacturer's protocol. The RNA concentration was diluted to a concentration of 500 ng/μl. Subsequently, the PrimeScript™ RT reagent kit with gDNA Eraser (cat. no. RR047A; Takara Bio, Inc.) was employed for RNA reverse transcription to generate cDNA according to the manufacturer's instructions. Specifically, the RT1 reaction system was composed of 2 μl RNA, 2 μl 5x gDNA eraser buffer, 1 μl gDNA eraser and 5 μl RNase-free H_2O. The RT2 reaction system consisted of 1 μl RT primer mix, 4 μl 5x primer buffer, 1 μl enzyme and 4 μl RNase-free H_2O. For the quantitative analysis of target mRNAs, including Cdk1, Clic6, Col11a1, Col1a1, Comp, Cxcl10, Fgf23, Gdf15, Gstp1, Igfbp2, Il1rn, Itgax, Itgbl1, Lama2, Mmp9, Serpine1, Trem2, Vcan, Akr1d1, Cxcl14, Enho, Pklr, Plin1, Pon3, Apoa4, Apoc2, Ccl20 and Gapdh, cDNA was amplified using quantitative PCR in a 20 μl TB green (cat. no. RR820A; Takara, Bio, Inc.) reaction mixture. After the reverse transcription products were placed on ice, quantitative PCR was performed using the Takara TB Green qPCR Master Mix kit. The reaction mixture for each reaction well was 20 μl, containing 10 μl TB Green, 0.2 μl forward primer, 0.2 μl reverse primer, 0.4 μl dye II, 7.2 μl ddH_2O and 2 μl cDNA. The thermocycling conditions for the reaction were as follows: 95˚C for 30 sec, followed by 40 cycles of amplification, with each cycle comprising 5 sec at 95˚C and 30 sec at 60˚C. RT-qPCR fluorescence detection was performed using an ABI7500 instrument (Thermo Fisher Scientific, Inc.). The reference gene, Gapdh was selected for the calculation of relative expression levels of each gene, utilizing the $2^{-\Delta\Delta Cq}$ method (51). Table SI provides a comprehensive overview of the primers utilized in the study.

Western blotting analysis. Liver tissue samples were prepared by grinding 100 mg of tissue in liquid nitrogen with RIPA buffer (cat. no. R0020; Beijing Solarbio Science & Technology Co., Ltd.). The lysate was thawed on ice for 30 min and centrifuged at 12,000 x g for 10 min at 4˚C. The resulting supernatant was collected and the protein concentration was quantified using a bicinchoninic acid assay kit (cat. no. PC0020; Beijing Solarbio Science & Technology Co., Ltd.). The protein samples (30 μg/well) were separated through 10% sodium dodecyl sulfate-polyacrylamide gel electrophoresis (cat. no. P1200; Beijing Solarbio Science & Technology Co., Ltd.) and transferred onto PVDF membranes (cat. no. IPVH00010; MilliporeSigma; Merck KGaA) utilizing a wet transfer technique. For blocking, membranes were incubated with a 7.5% solution of skim milk (cat. no. P0216; Beijing Solarbio Science & Technology Co., Ltd.) in 1x TBST (0.1% Tween-20; cat. no. T1082; Beijing Solarbio Science & Technology Co., Ltd.) for 2 h at room temperature. The specific bands were subsequently excised based on the target molecular weight and then incubated with primary antibodies against Plasminogen activator inhibitor-1 (PAI-1; 1:1,000; cat. no. 13801-1-AP; Proteintech Group, Inc.), Matrix metalloproteinase-9 (MMP-9; 1:500; cat. no. 27306-1-AP; Proteintech Group, Inc.) Glutathione S-transferase P1 (GSTP1; 1:5,000; cat. no. bs-1100r; Proteintech Group, Inc.) and Glyceraldehyde-3-phosphate dehydrogenase (GAPDH; 1:12,000; cat. no. 60004-1-Ig; Proteintech Group, Inc.) overnight at 4˚C. GAPDH was used as the internal control. The membrane was then washed three times with 1x TBST (0.1% Tween-20) for 10 min/wash. The anti-rabbit immunoglobulin G and horseradish peroxidase-linked secondary antibodies (1:2,000; cat. no. 7074S; CST Biological Reagents Co., Ltd.) were diluted in 5% skim milk solution in 1x TBST (0.1% Tween-20 used in TBST) and applied to the membranes for 1 h at room temperature. The. Next, the membrane was washed three times with 1x TBST for 10 min each time. After treating the membrane with the ECL Plus working solution (cat. no. BL520A; Labgic Technology Co., Ltd.) for 5 min, it was placed in a dark container and sealed. The visualization of protein expression was performed using the FluorChem E system (ProteinSimple). The signal intensities of bands were quantified using ImageJ 1.8.0 (National Institutes of Health).

ELISA for serum. ELISA kits were used to quantify the concentrations of PAI-1 (cat. no. JL12416; Shanghai Jianglai Biological Technology Co., Ltd.), MMP-9 (cat. no. PM733; Beyotime Institute of Biotechnology) and GSTP1 (cat. no. E1090m; EIAab Science, Inc.) within the serum of the study subjects, according to the manufacturer's protocols. The values for the research samples were ascertained through the establishment of a calibration standard using standard serial solutions. The resultant data were presented in units of pg/ml or ng/ml.

Cell culture and induced fatty liver cells. HepG2 cells (cat. no. CL-0103; Procell Life Science&Technology Co., Ltd.) were cultured into 12-well plates at a density of $4x10^4$ in a controlled environment using DMEM supplemented with 10% FBS (cat. no. C2810-0050X10; Shanghai VivaCell Biosciences, Ltd.) and 100 U/ml penicillin plus 100 μg/ml streptomycin (cat. no. C0222; Beyotime Institute of Biotechnology). The culture conditions maintained a constant temperature of 37˚C, a 5% CO_2 atmosphere and a pH of 7.2-7.4.

The treatment solutions for free fatty acids (FFAs) were prepared by combining palmitic acid (PA; cat. no. P0500, MilliporeSigma) and oleic acid (OA; O1383; MilliporeSigma) in a 1:2 molar ratio of respectively. The stock solutions of PA (78 mM) and OA (354 mM) in DMSO were stored at -20˚C until needed. FFA solutions with concentrations created by mixing the stock solutions of PA and OA at a 1:2 (PA:OA) ratio in DMEM. HepG2 cells were exposed to FFAs at concentrations of either 200 or 500 μM for a duration of 24 h at 37˚C with the aim of inducing hepatic steatosis.

Cell immunofluorescence. For the immunofluorescence assays, HepG2 cells were initially seeded onto glass coverslips at a density of $5x10^4$ cells/cm^2 and allowed to adhere for a minimum of 6 h. Subsequently, the cells were fixed using a 4% paraformaldehyde solution (cat. no. BL539A; Biosharp Life Sciences) for 20 min at room temperature. After being rinsed thrice with PBS, the cells were incubated in 0.01% Triton-X100-containing PBS for 15 min at room temperature, followed by another incubation in a PBS solution containing 1% BSA and 10% normal goat serum (cat. no. B900780; Proteintech Group, Inc.) for 45 min at room temperature. Subsequently, the cells were incubated overnight at 4˚C with primary polyclonal antibodies against PAI-1 (1:400 in PBS; cat. no. 13801-1-AP; Proteintech Group, Inc.) and MMP-9 (1:400 in PBS; cat. no. 13801-1-AP; Proteintech Group, Inc.). The coverslips were rinsed with PBS and then incubated with CoraLite488-conjugated goat anti-rabbit immunoglobulin G (1:600 in PBS; cat. no. SA00013; Proteintech Group, Inc.) for 1 h at room temperature. Following two additional washes with PBS, the cells were incubated with DAPI (1:200 in PBS; cat. no. C1002; Beyotime Institute of Biotechnology) for 20 min at room temperature and rinsed twice more in PBS. Finally, the coverslips were mounted on standard slides using AntiFade mounting medium (cat. no. HY-K1042; MedChemExpress). HepG2 cells that were immunolabeled for PAI-1 and MMP-9 were imaged using a confocal TCS SP5 fluorescence microscope (Leica Microsystems GmbH).

ELISA for cell supernatant. In the present study, ELISA kits were utilized to quantify the levels of PAI-1 (cat. no. JL12941; Shanghai Jianglai Biological Technology Co., Ltd.) and MMP-9 (cat. no. PM738; Beyotime Institute of Biotechnology) in the cell supernatant. The quantification process was performed according to the manufacturer's protocols and values of the samples were determined with reference to a calibration curve. This curve was established through serial dilution of known standards. The results were presented in units of pg/ml or ng/ml.

Statistical analysis. Continuous variables were presented as the mean ± SD. Unpaired Student's t-test or Mann-Whitney U test was employed to compare differences between groups in cases of parametric and non-parametric data, respectively. For group data analysis, one-way ANOVA with Tukey's post hoc test or Kruskal-Wallis test with Dunn's post hoc test were applied as appropriate. P<0.05 was considered to indicate a statistically significant difference. All statistical analyses were performed using GraphPad 8.0 software (Dotmatics). Receiver operating characteristic (ROC) curves were obtained using R package pROC (version 1.18.4; https://rdocumentation.org/packages/pROC/versions/1.18.4).

Results

HFFD feeding induces increased levels of cholesterol and triglycerides and decreases insulin sensitivity. At the commencement of the present study, the mean body weight of mice in the chow-fed and HFFD-fed groups was 18.60±1.55 and 18.63±1.62 g, respectively. However, as the experiment progressed, the body weight of the HFFD-fed mice exhibited a statistically significant increase in comparison with that of the chow-fed mice. This significant difference became evident after 6 weeks of HFFD treatment (HFFD: 36.26±2.09 g vs. chow: 29.66±2.30 g; P<0.05). This disparity in body weight between the two groups persisted throughout the rest of the 22-week study period (Fig. 1A). Upon being fed the HFFD, the mice developed a distinct phenotype characterized by obesity, along with obesity-associated high cholesterol and metabolic imbalances involving triglycerides and insulin (Fig. 1B-F). These parameters exhibited a notable and sustained increase over the course of the experiment, from week 6 to 22. While blood glucose levels showed a significant increase from 14 weeks (P<0.05) (Fig. 1G), mice on the HFFD displayed a significant rise in serum insulin levels starting from the 10th week, and this sustained elevation continued until the 22nd week (P<0.05). Furthermore, mice fed the HFFD demonstrated the development of insulin resistance between week 10 and 22, as indicated by analysis of the HOMA index (P<0.05; Fig. 1H and I).

HFFD leads to hepatocellular injury and lipid deposition within the liver. Beyond week 14, animals fed with the HFFD exhibited significantly higher liver weights compared with those fed the chow diet (Fig. 2A). Concurrently, an increase in the serum levels of hepatic dysfunction markers, ALT and AST, were closely associated with the onset of obesity following HFFD feeding. Particularly noteworthy was the rapid and significant elevation in plasma ALT and AST levels observed from 10 weeks in HFFD-fed mice in comparison with their chow-fed counterparts (P<0.05; Fig. 2B and C). A biochemical analysis of intrahepatic lipids demonstrated a significant rise in liver cholesterol levels from week 14 in mice subjected to the HFFD (P<0.05); however, the control group maintained consistently lower liver cholesterol levels throughout the duration of the study (Fig. 2D). Furthermore, liver triglyceride levels were markedly elevated in the HFFD-fed mice at week 10 compared with the chow-fed mice, and this trend and disparity persisted throughout the rest of the study (P<0.05). Conversely, the control group exhibited minimal changes in hepatic triglyceride levels throughout the study (Fig. 2E). NEFA levels exhibited a substantial surge after the 6th week and remained significantly elevated during all subsequent time points (P<0.05) in the HFFD-fed group compared with the control group. The control group maintained relatively stable NEFA levels throughout the study period (Fig. 2F). Feeding with the HFFD triggered the development of NAFLD, which progressively evolved into NASH over the extended study period.

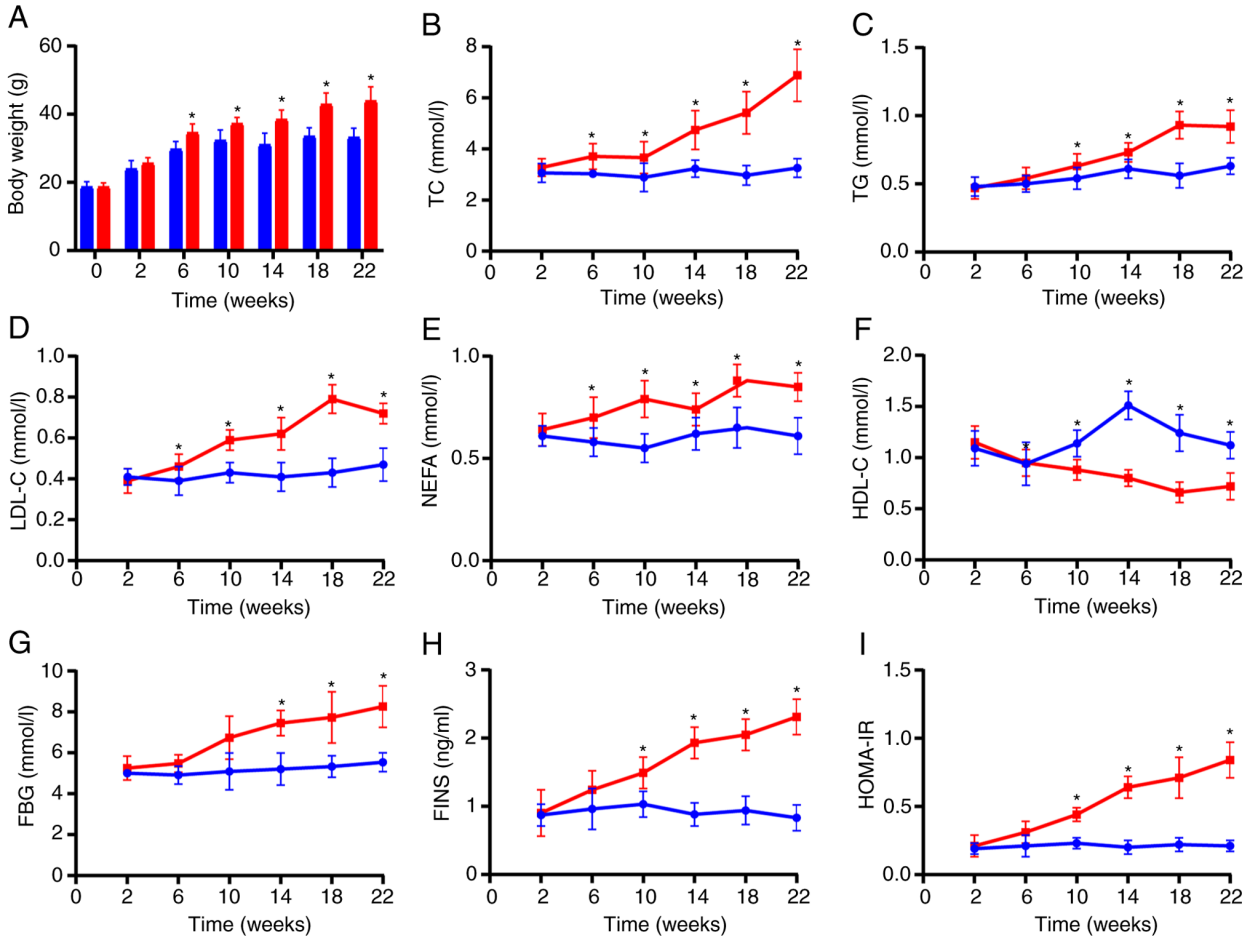

Figure 1. Feeding with HFFD induces increased levels of cholesterol and triglycerides and reduced insulin sensitivity. Effect of HFFD feeding and chow feeding on (A) body weight and serum levels of (B) TC, (C) TG, (D) LDL-C, (E) NEFA, (F) HDL-C, (G) FBG, (H) FINS and (I) HOMA-IR index. Blue represents chow-fed mice; red represents HFFD-fed mice. Data are presented as the mean ± SD (n=6), *P<0.05 vs. chow-fed. HFFD, high-fat and fructose diet; TC, total cholesterol; TG, triglycerides; LDC-C, low-density lipoprotein cholesterol; NEFA, non-esterified fatty acids; HDL-C, high-density lipoprotein cholesterol; FBG, fasting blood glucose; FINS, fasting serum insulin; HOMA-IR, homeostatic model assessment for insulin resistance.

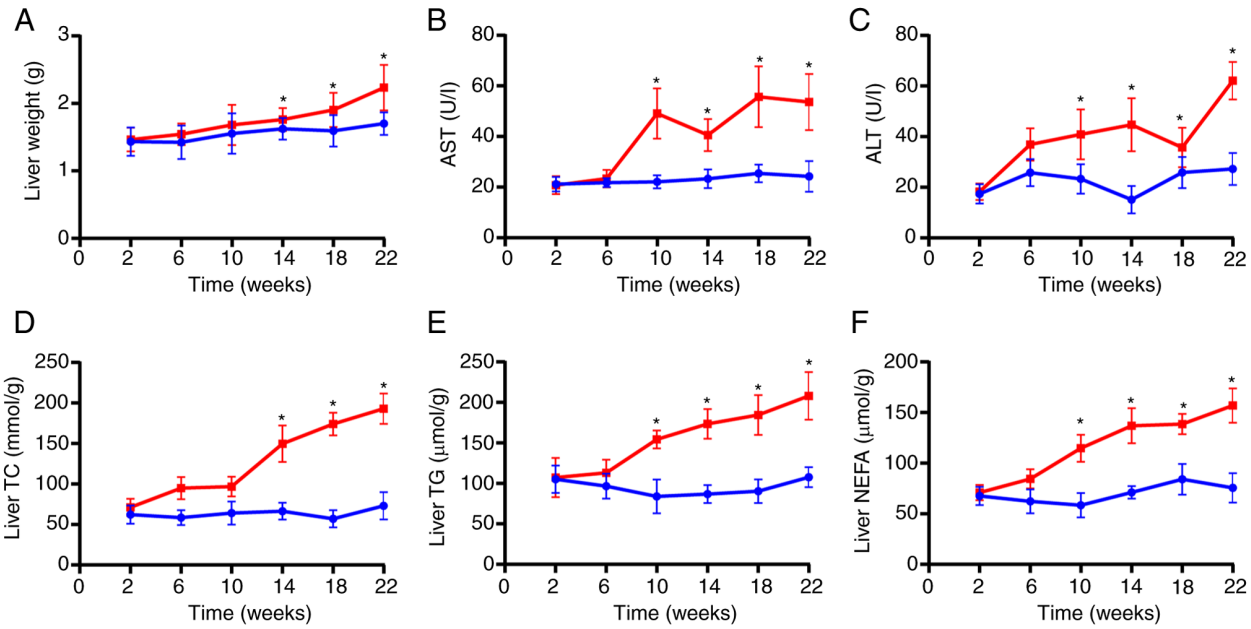

Figure 2. Effect of HFFD feeding and chow feeding on hepatic features. (A) Liver weight and levels of (B) AST and (C) ALT. Levels of intrahepatic (D) TC, (E) TG and (F) NEFA. Blue represents chow-fed mice; red represents HFFD-fed mice. Data are presented as the mean ± SD (n=6), *P<0.05 vs. chow-fed. HFFD, high-fat and fructose diet; TC, total cholesterol; TG, triglycerides; NEFA, non-esterified fatty acids; AST, aspartate aminotransferase; ALT, alanine aminotransferase.

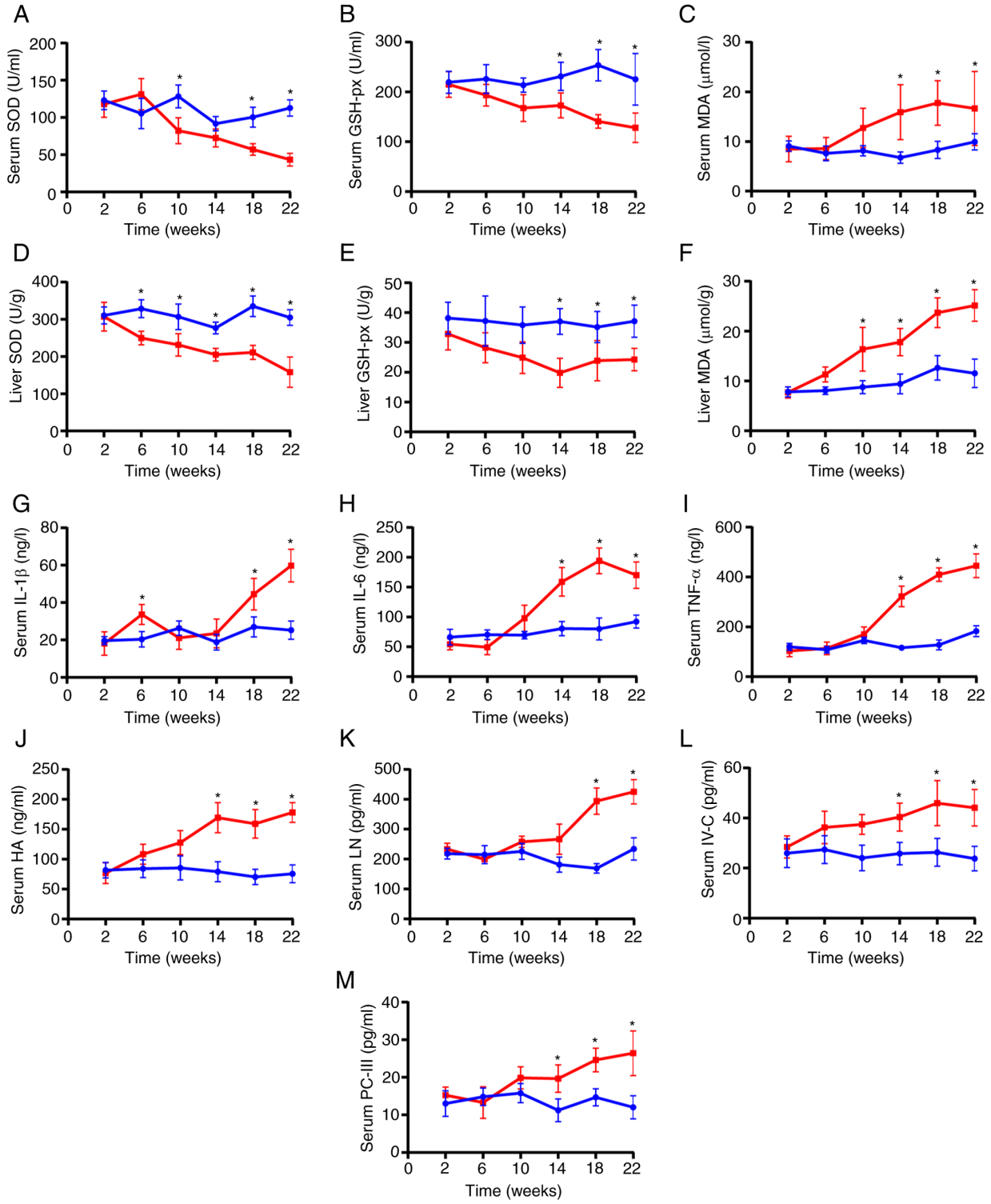

Figure 3. Effect of a HFFD and chow diet on oxidative stress, inflammation and pro-fibrogenesis. Quantification of oxidative stress indicators in serum, including (A) SOD, (B) GSH-px and (C) MDA, and liver (D) SOD, (E) GSH-px and (F) MDA. Quantification of inflammatory factors including (G) IL-1β, (H) IL-6 and (I) TNF-α in serum. Quantification of liver fibrosis-related serum markers, including (J) HA, (K) LN, (L) IV-C and (M) PC-III levels. Blue represents chow-fed mice; red represents HFFD-fed mice. Data are presented as the mean ± SD (n=6), *P<0.05 vs. chow-fed. HFFD, high-fat and fructose diet; SOD, superoxide dismutase; GSH-px, glutathione peroxidase; MDA, malondialdehyde; HA, hyaluronic acid; LA, laminin; IV-C, type IV collagen; PC-III, type III procollagen.

HFFD feeding induces oxidative stress, inflammation and profibrogenic. To evaluate the effect of a HFFD on oxidative stress, the activities of antioxidant enzymes that shield cells from ROS-induced damage, SOD and GSH-Px, along with levels of MDA, a marker of lipid peroxidation, were assessed in both serum and liver tissue. The findings indicated a significant reduction in the activities of both SOD (at 10, 18 and 22 weeks, P<0.05) and GSH-Px (at 14, 18 and 22 weeks, P<0.05), accompanied by a rapid increase in MDA levels (from week 14 onward, P<0.05) in the serum of HFFD-fed

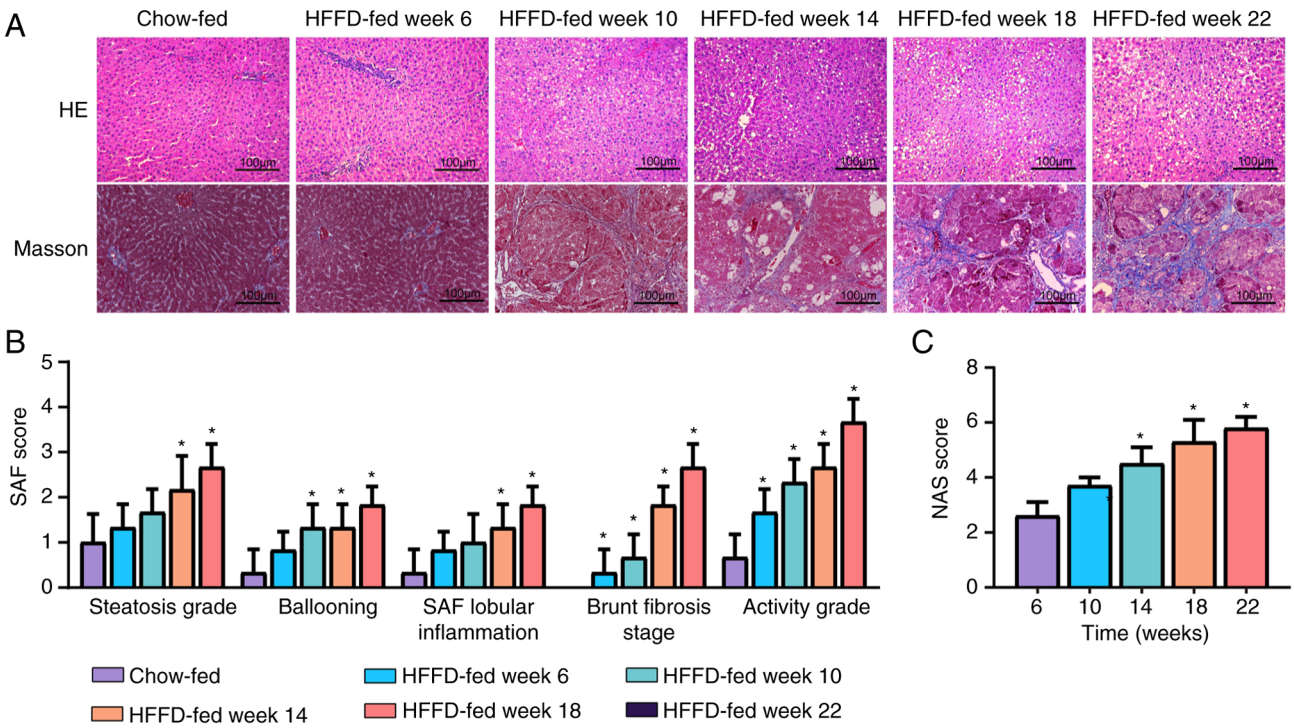

Figure 4. Effect of a HFFD and chow diet on histopathologic analysis of hepatic tissue. (A) H&E staining and Masson staining (magnification, x400). (B) SAF and (C) NAS score. Data are presented as the mean ± SD (n=3), *P<0.05 vs. chow-fed. HFFD, high-fat and fructose diet; SAF, steatosis, activity and fibrosis; NASH, nonalcoholic steatohepatitis; NAS, NASH activity score; HE, H&E staining.

animals in comparison with the chow-fed mice (Fig. 3A-C). The imbalance of oxidative stress in the liver of mice with HFFD intervention began to manifest significantly (P<0.05) at 14 weeks (Fig. 3D-F). These results indicated an elevation in oxidative stress. Furthermore, the inflammatory response was evaluated by measuring the concentrations of IL-6, IL-1β and TNF-α in serum using ELISA. The results revealed a significant increase in IL-1β levels at weeks 6, 18 and 22 (P<0.05) in HFFD-fed animals (Fig. 3H), while IL-6 levels peaked at week 18 and exhibited a slight decline by week 22 (P<0.05; Fig. 3G). Moreover, TNF-α levels displayed a substantial increase at week 14 and remained elevated throughout the study (P<0.05; Fig. 3I). Serum markers associated with liver fibrosis, including HA, LN, PC-III and IV-C, exhibited significant increases (P<0.05) in HFFD-fed animals compared with the control group (Fig. 3J-M). Notably, HA, PC-III and IV-C demonstrated significant differences after 14 weeks of HFFD intervention, with a slower rate of increase. There was a pronounced and significant rise in LN concentration by the 18th week. From week 14 to 22, a marked increase was observed in all these parameters, which indicated a progressive worsening of hepatic oxidative stress, inflammation and fibrosis throughout the feeding period.

HFFD feeding induces alterations in liver morphology. Liver tissues were collected from all groups at 6, 10, 14, 18 and 22 weeks. These collected tissues were subjected to histological examination using hematoxylin and eosin, and Masson staining. In the chow-fed group, the hepatic lobule structure displayed clarity, with hepatic cords exhibiting organized radial arrangements extending from the central vein to the surrounding area. Minimal lipid deposition was observed in hepatocytes and there was no significant collagen hyperplasia. Only a few Kupffer cells were detected in the hepatic sinusoids. In contrast, liver tissue from HFFD-fed animals exhibited notable morphological alterations, including an inflammatory response, fatty degeneration and cellular necrobiosis when compared with the normal lobe of mice in the control group. Starting from week 14, fibroblasts were identified between the interlobular and portal areas, accompanied by bubble-like degeneration and necrosis. Observations indicated an increase in fibroblast count and remodeling of the hepatic lobe between weeks 14 and 22 (Fig. 4A), along with gradually rising SAF and NAS scores when compared with the chow-fed group (Fig. 4B and C). Additionally, Masson staining (Fig. 4A) from weeks 18 and 22 indicated increasing levels of collagen deposition and fibrosis accumulation within the hepatic tissue of animals fed with HFFD.

Defining DEG sets associated with NASH progression. To identify genes that are differentially expressed and participated in the development of NASH and liver fibrosis, as well as to assess the temporal regulation of gene signatures during the course of disease progression, high-throughput sequencing analysis of hepatic gene expression was performed. As the livers of mice at week 6 yielded a relatively small number of DEGs compared with the chow-fed group, the analysis of DEGs was deferred until week 10. The HFFD diet significantly increased the number of DEGs, with 304-409 DEGs identified when comparing individual time points between weeks 10-22 (Fig. 5E). GO annotation analysis of DEGs (Fig. 5A-D) after 10-22 weeks of HFFD intervention revealed that early in the HFFD intervention (at 10 and 14 weeks) biological processes primarily involved metabolic and inflammatory reactions.

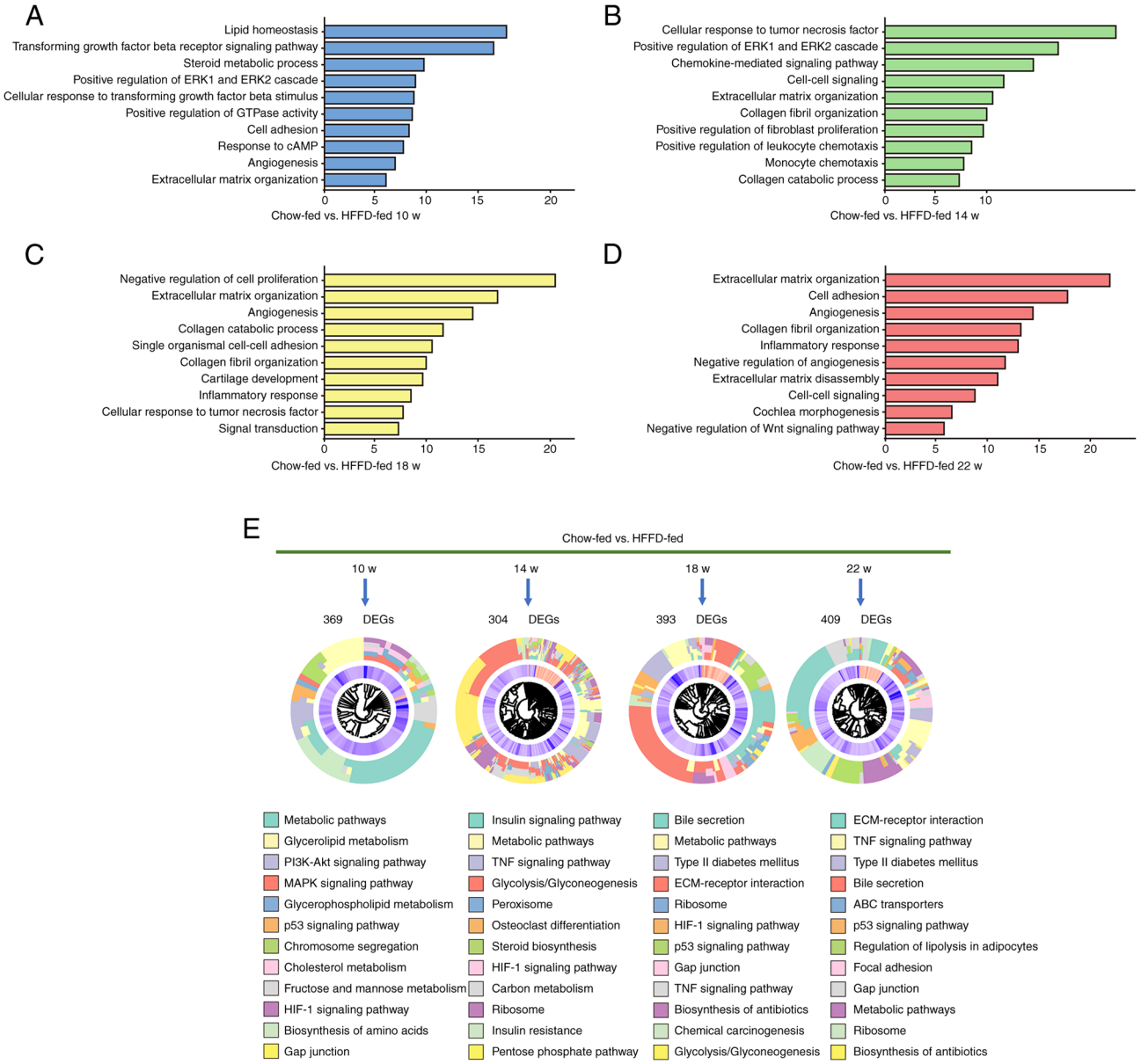

Figure 5. GO enrichment analysis and KEGG analysis of DEGs after HFFD intervention at different time points in mice. (A-D) GO annotation pairwise analysis comparing HFFD-fed mice with chow-fed mice. The RNA-seq data were subjected to pairwise analysis, identifying DEGs that were then analyzed for GO annotation enrichment using cluster Profiler R package. In addition, (E) KEGG pathway enrichment was carried out to compare HFFD-fed mice with chow-fed mice using the DEGs at each time point. The cluster Profiler R package annotation tool was employed and the top 12 enriched pathways were listed for each analysis based on their P-value. The results are presented in-log10(P-value) format. HFFD, high-fat and fructose diet; GO, gene ontology; KEGG, Kyoto Encyclopedia of Genes and Genomes; DEGs, differentially expressed genes.

These processes included 'steroid metabolic process', 'transforming growth factor β receptor signaling pathway', 'lipid homeostasis', 'cellular response to tumor necrosis factor', 'positive regulation of ERK1 and ERK2 cascade' and 'chemokine-mediated signaling pathway'. In contrast, HFFD feeding induced collagen and fiber-associated processes at 18 and 22 weeks, including 'negative regulation of cell proliferation', 'extracellular matrix (ECM) organization', 'angiogenesis' and 'collagen fibril organization'. A marked proportion of genes that displayed differential expression at week 14 exhibited sustained differential regulation during weeks 18 and 22. The Kyoto Encyclopedia of Genes and Genomes (KEGG) pathway enrichment analysis supported the findings of the GO enrichment analysis. By week 10 of HFFD treatment, pathways related to NASH and liver fibrosis showed modulation, as evidenced by marked enrichment in these pathways. This was exemplified by changes in gene expression associated with lipid catabolism pathways, robust activation of genes involved in inflammation signaling pathways and hepatic fibrosis activation. The top canonical pathways were primarily enriched in disease progression characteristics, such as dysregulation of lipid metabolism, hepatic cellular inflammation and injury, increased ECM production and impaired degradation in the liver (Fig. 5E).

Dynamics of core genes involved in NASH progression. To identify a set of core genes associated with the transition from the initial stages of NASH to a more advanced phase

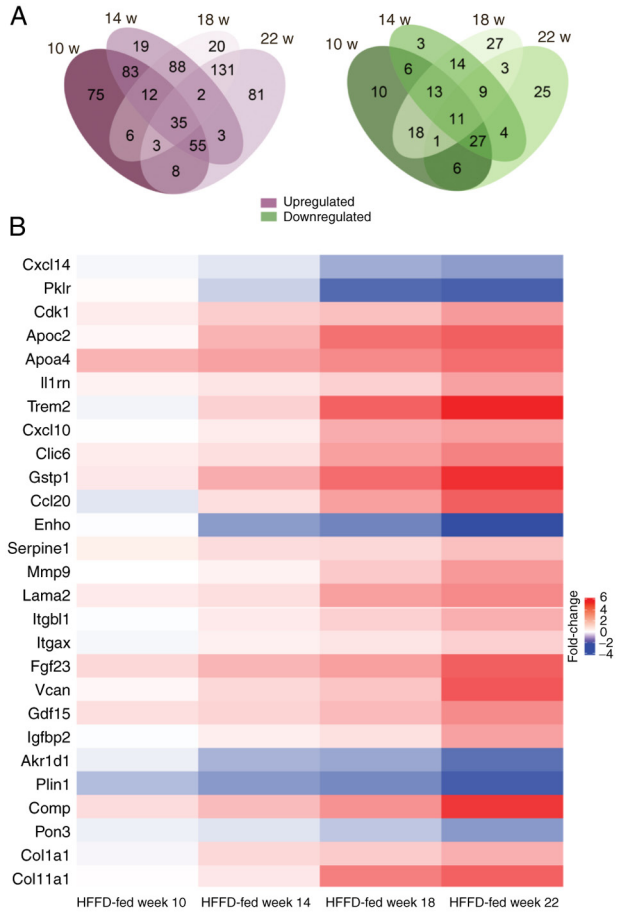

Figure 6. Dynamic gene alterations in the progression of mouse models of NASH. (A) Venn diagram of the overlap in differential expression in the HFFD-fed mice at different time points compared with the chow-fed mice. (B) Heatmap of 27 significantly regulated genes in the livers of mice with HFFD intervention for 10, 14, 18 and 22 weeks. The expression fold change is compared with that in chow-fed mice. HFFD, high-fat and fructose diet; NASH, nonalcoholic steatohepatitis.

of the disease, the overlap of DEGs across various pairwise comparisons was assessed. The overlap between DEGs at each time point group was compared with one another using Venn diagrams. The intersections of DEGs at weeks 10, 14, 18 and 22, when compared with the chow-fed baseline, indicated 46 significantly altered genes (35 upregulated and 11 downregulated) in mice with NASH (Fig. 6A). Proteins that could be secreted into the bloodstream based on the DEGs in the Protein Atlas database were also considered. According to the HPA database, among a total of 45 genes, 27 were found to encode secretory proteins which can be detected in the blood. These genes were categorized as potential blood-based biomarkers capable of distinguishing between different stages of NASH in mice with NAFLD. Among these genes, 21 exhibited a gradual increase in expression with the progression of the disease (Cdk1, Clic6, Col11a1, Col1a1, Comp, Cxcl10, Fgf23, Gdf15, Gstp1, Igfbp2, Il1rn, Itgax, Itgbl1, Lama2, Mmp9, Serpine1, Trem2, Vcan, Ccl20, Apoa4 and Apoc2), while 6 genes showed a gradual decrease (Akr1d1, Cxcl14, Enho, Pklr, Plin1 and Pon3; Fig. 6B).

Verification of the core genes employing a GEO dataset. Within the core gene set, a group of genes with distinct roles were identified. Based on GO and KEGG analysis, Vcan, Serpine1, Mmp9, Lama2, Itgbl1, Itgax, Fgf23, Comp, Col1a1 and Col11a1 are linked to 'extracellular matrix (ECM) organization'. Trem2, Igfbp2, Gstp1, Apoc2, Apoa4, Pklr, Enho, Pon3, Plin1, and Akr1d1 contribute to 'steroid metabolic process' and 'lipid homeostasis'. Il1rn, Gdf15, Cxcl10, Clic6, Cdk1 and Ccl20 serve crucial roles in 'response to stimulus'. These biological processes are widely recognized as significant drivers of hepatic fibrogenesis and steatosis, which are key pathological events in various liver diseases.

To evaluate the predictive potential of the core genes in individuals with NAFLD from the discovery cohort (GSE135251), receiver operating characteristic (ROC) analysis was used as the primary statistical technique. The performance of the ROC curves was assessed using the area under the curve (AUC). In the models predicting steatohepatitis grade (Fig. 7A), Gstp1 (area Under the Receiver Operating Characteristic curve, AUROC=0.8414; P<0.0001), Trem2 (AUROC=0.8283; P<0.0001) and Serpine1 (AUROC=0.8007; P<0.0001) expression were significant independent variables that accurately predicted NAS ≥4. Moreover, Itgbl1, Clic6, Plin1, Lama2, Fgf23, Comp, Ccl20, Akr1d1, Cxcl10, Col1a1, Enho and Cdk1 also performed well, with AUC values >0.7. In the prediction of an SAF activity score of ≥2 (Fig. 7B), Serpine1 (AUROC=0.8544; P<0.0001), Fgf23 (AUROC=0.8182; P<0.0001), Ccl20 (AUROC=0.8125; P<0.0001), Trem2 (AUROC=0.8088; P<0.0001), Mmp9 (AUROC=0.8053; P<0.0001) and Gstp1 (AUROC= 0.8037; P<0.0001) expression were statistically significant. Furthermore, Gdf15, Cxcl14, Clic6, Akr1d1, Lama2, Pklr, Col1a1, Comp, Enho, Vcan, Plin1, Col11a1 and Pon3 also demonstrated good performance, with AUC values >0.7. These findings highlighted the diagnostic value of the core genes associated with disease progression and dynamic changes in the early phase of human NASH.

Validation of core genes in mouse livers. The core genes associated with liver tissue from NASH and control mice were validated using RT-qPCR. The results demonstrated significant increases in the mRNA expression levels of Ccl20, Cdk1, Clic6, Col1a1, Comp, Cxcl10, Fgf23, Gdf15, Gstp1, Igfbp2, Il1rn, Itgax, Itgbl1, Lama2, Mmp9, Serpine1, Trem2 and Vcan in HFFD-fed mice. However, Cxcl14, Enho, Pklr, Plin1 and Pon3 exhibited reduced expression compared with that in chow-fed mice (Fig. 8). By aggregating expression data from all time points, a time-resolved response of processes, including metabolism, inflammation and fibrosis, that contribute to the emergence of NASH and fibrotic changes in the liver was observed. Animals fed a HFFD for 6, 10 or 14 weeks displayed regulatory patterns in lipid metabolism and inflammation networks when compared with healthy counterparts. Notably, the lipid metabolism pathway was the first to be triggered, with activation starting at week 6. In contrast, inflammation-related genes became activated from week 10 onward, and fibrosis-related genes showed significant upregulation at 18 and 22 weeks.

Verification of protein expression of core genes in the liver. To evaluate the gene expression of core genes at the protein level, western blotting analyses were performed to identify significant changes in protein expression levels. These changes were

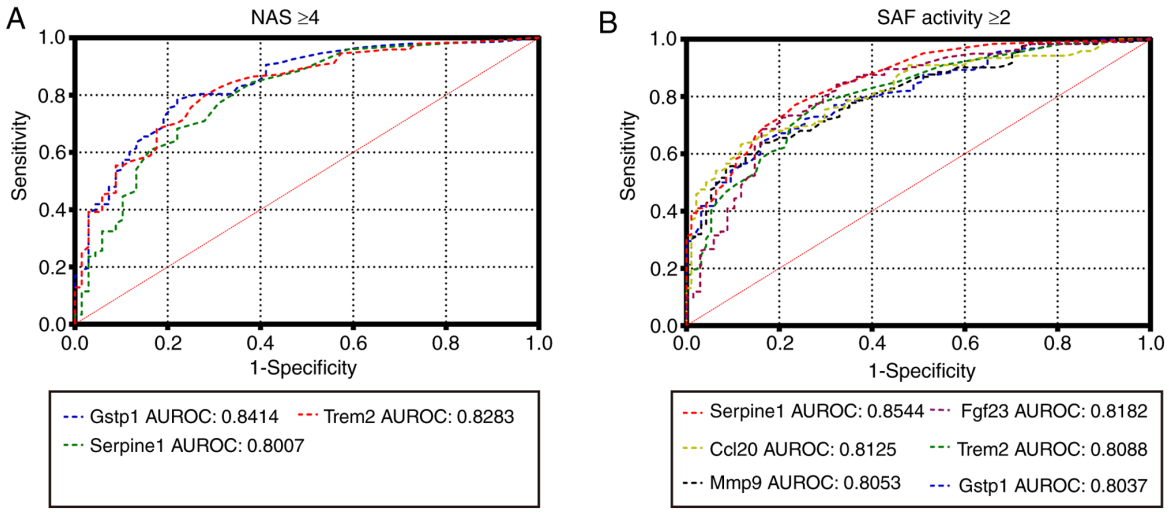

Figure 7. The predictive potential of core genes in the NAFLD discovery cohort (GSE135251) using ROC analysis. ROC curves show the specificity and sensitivity of the hub genes as biomarkers to recognize (A) NAS ≥4 and (B) SAF activity score ≥2. NAFLD, nonalcoholic fatty liver disease; AUROC, area under the receiver operating characteristic curve.

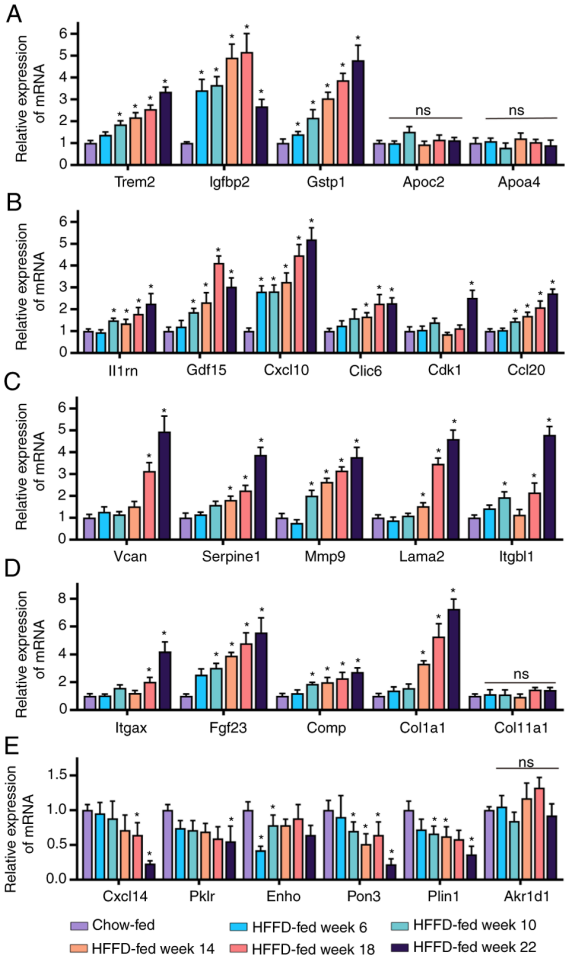

Figure 8. Alterations in the hepatic gene expression profile of mice subjected to long-term HFFD. The genes included in the upregulated and downregulated gene sets were assessed by RT-qPCR. Among them, upregulated genes mainly regulate (A) metabolism (Trem2, Igfbp2, Gstp1, Apoc2 and Apoa4), (B) inflammation (Il1rn, Gdf15, Cxcl10, Clic6, Cdk1 and Ccl20) and (C and D) fibrotic processes (Vcan, Serpine1, Mmp9, Lama2, Itgbl1, Itgax, Fgf23, Comp, Col1a1 and Col11a1), while downregulated genes mainly affect (E) metabolism and the inflammatory response (Cxcl14, Pklr, Enho, Pon3, Plin1 and Akr1d1). Data are presented as the mean ± SD (n=3), *P<0.05 vs. chow-fed. HFFD, high-fat and fructose diet; ns, not significant.

identified based on the high AUC values obtained from ROC analysis of mice subjected to a HFFD diet. The protein levels of PAI-1 (a secreted protein encoded by Serpine1), MMP-9 and GSTP1 were notably increased in HFFD-fed mice, however, no significant changes were observed before the 14-week time point when compared with the corresponding controls (Fig. 9A-D). Furthermore, the concentrations of PAI-1 and MMP-9 proteins in the serum of mice were quantified, which demonstrated an increase (P<0.05) in both proteins with the longer duration of high-fat diet intervention (Fig. 9E-G).

The present study was designed to investigate the correlation between PAI-1 and MMP-9 levels and the severity of NAFLD. This was achieved by evaluating their potential as noninvasive serum biomarkers, aiming to distinguish between control mice and mice with NAFLD. The results demonstrated an association between serum PAI-1 levels and NAS. Furthermore, a significant association between PAI-1 levels, steatosis and hepatocyte ballooning was observed. However, no association was found with inflammation, (Fig. 9H). This pattern of findings strongly implied that heightened serum PAI-1 levels could potentially serve as an indicator of liver damage, characterized histologically by lipidosis. Similarly, the gradual increase in serum MMP-9 levels, (Fig. 9I) as steatosis and inflammation progressed, rather than hepatocyte ballooning, underscored that serum MMP-9 levels mirror hepatocellular injury stemming from lipid accumulation in the liver during the progression of NASH. In summary, the results indicated that elevated levels of PAI-1 and MMP-9 could be linked to the transition from steatosis to NASH and could potentially contribute to the onset of hepatic fibrosis.

Validation of hub genes in vitro. To obtain a more comprehensive understanding of the mechanisms driving NAFLD progression, alterations in the protein expression patterns of PAI-1 and MMP-9 *in vitro* were examined by subjecting HepG2 cells to lipid loading (at 200 and 500 μmol FFAs). Following 24 h of treatment, a significant increase in PAI-1

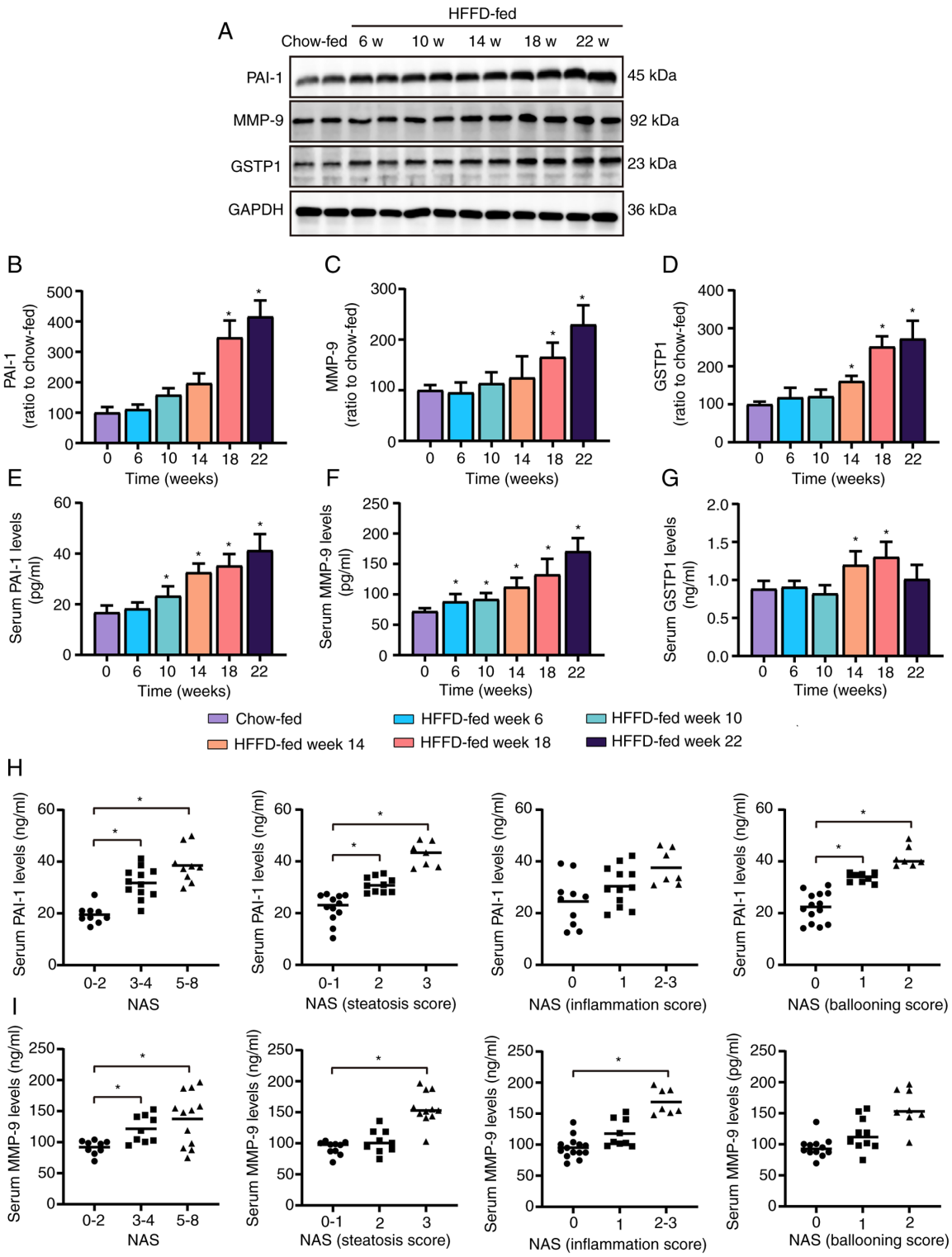

Figure 9. Levels of relevant proteins in the liver and serum of mice under long-term intervention with a HFFD. (A) The protein expression levels of PAI-1, MMP-9 and GSTP1 in HFFD-fed mice and corresponding chow-fed mice by Western blotting analysis with quantification (n=3). (B-D) The band intensity ratios were analyzed by ImageJ. (E-G) ELISA readout for PAI-1, MMP-9 and GSTP1 in the serum of chow-fed or HFFD-fed mice (n=6). Data are presented as the mean ± SD. (H) The NAS score was used to determine the relative serum levels of PAI-1, steatosis, inflammation and ballooning scores of the NAS. (I) The NAS score was used to determine the relative serum levels of MMP-9 and steatosis, inflammation and ballooning scores of the NAS. *P<0.05. NASH, nonalcoholic steatohepatitis; NAS, NASH activity score; HFFD, high-fat and fructose diet.

protein expression levels (P<0.05) were observed, compared with the control, in both intracellular and secretory compartments when HepG2 cells were exposed to 500 μmol FFAs (Fig. 10A-C). Additionally, a substantial elevation in MMP-9 protein levels (P<0.05) at both concentrations (Fig. 9D-F) was noted, compared with the control. These results reinforced the potential of PAI-1 and MMP-9 as biomarkers for the diagnosis and monitoring of NAFLD progression.

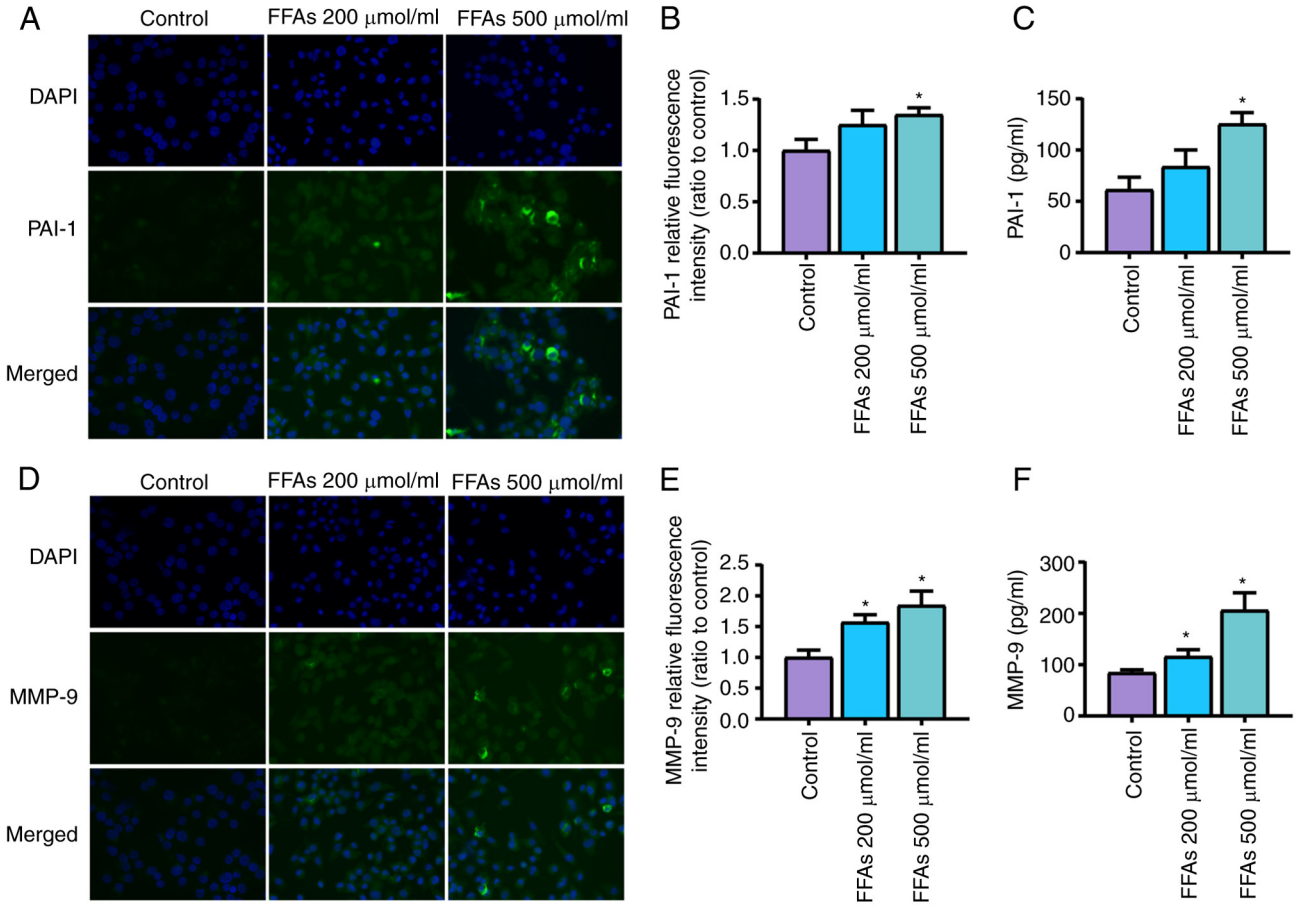

Figure 10. Expression of PAI-1 and MMP-9 in HepG2 cells treated with FFAs. Immunofluorescence staining for (A) PAI-1 and (D) MMP-9 in HepG2 cells exposed to different FFA concentrations (200 and 500 μmol). Nuclei were counterstained with DAPI and, (B) PAI-1+ and (E) MMP-9+ were semi-quantified and compared using an inverted microscope (magnification, x400). (C) PAI-1 and (F) MMP-9 concentrations in the cell supernatant by ELISA. Data are presented as the mean ± SD. *P<0.05. FFA, free fatty acid.

Discussion

In the present analysis, a transcriptomics framework was used to evaluate liver tissue collected from mice with histologically confirmed NAFLD. The primary objective was to identify genes associated with fibrosis and to establish a panel for detecting the disease in adults with a heightened risk for NASH. This subgroup constitutes a minority of patients with NAFLD who also exhibit advanced liver fibrosis, posing a significant risk for complications stemming from prolonged hepatic dysfunction (52). The progression of NASH and the development of liver fibrosis is a gradual process occurring over an extended period (39). However, our understanding of this process remains limited because clinical symptoms typically emerge only in the advanced stages of disease, making it challenging to investigate early molecular mechanisms of disease progression in humans (53,54). By contrast, NASH animal models offer insights into time-resolved events and provide crucial information regarding early processes contributing to disease onset (55). Therefore, the mouse model employed in the present study holds important translational relevance and the findings of the present study hold significance in addressing the health challenges posed by NAFLD and in preventing the progression to NASH.

Numerous animal models have been employed to study the development of NASH and explore relevant biomarkers reflecting liver pathology (56-58). However, none of these models perfectly replicate the complete array of molecular mechanisms implicated in human disease. Among the available models, HFFD-induced models have emerged as promising tools for studying NASH and fibrosis, offering a more comprehensive and physiologically relevant milieu. These models mimic key characteristics of metabolic syndrome seen in humans, including adiposity, hyperlipidemia and insulin insensitivity (59). HFFD-fed mice are preferred over chemically induced fibrosis models (such as carbon tetrachloride), as they manifest features of dysmetabolic syndrome, characterized by adiposity, high cholesterol, high triglycerides and impaired insulin sensitivity (60). Mice fed a HFFD exhibited liver damage, as indicated by elevated serum ALT and AST levels compared with those on a regular chow diet. Histopathological analysis confirmed the progressive increase in hepatic lipid accumulation, cellular hypertrophy, inflammation and hepatic perisinusoidal fibrosis over time. Moreover, oxidative stress and inflammation have been recognized as important mechanisms linking obesity and metabolic disorders (61). The present study revealed that as the duration of high-fat diet intervention increased, oxidative stress levels in both serum

and liver increased significantly, along with the production of inflammatory factors in serum, which was particularly evident at the 14-week time point when substantial liver pathological damage was observed. Notably, by integrating transcriptomics with histopathology, the temporal sequence of core genes involved in the progression of the disease from mild hepatic steatosis to NASH, with or without liver fibrosis was identified. These findings contribute to an enhanced understanding of the pathogenic mechanisms underlying disease initiation and advancement, as well as the prompt identification of pathological pathways which lead to hepatic fibrosis. Furthermore, these insights can guide the development of techniques aimed at uncovering circulating markers for hepatic fibrosis. Overall, owing to its ability to replicate metabolic syndrome characteristics and induce progressive liver damage and fibrosis, the HFFD mouse model serves as a suitable representation of human NASH accompanied by hepatic fibrosis (62).

The current paradigm for disease biomarker discovery predominantly relies on the detection of molecular differences between normal and pathological states. However, due to the varying stages and heterogeneous progression of NAFLD, distinguishing between simple hepatic steatosis and NASH poses a significant challenge (63). By analyzing large-scale datasets and integrating genomics, transcriptomics, proteomics and metabolomics, researchers can gain a more comprehensive understanding of the disease and identify novel diagnostic and therapeutic targets, as evidenced by in-depth knowledge about the molecular pathways responsible for the development of human diseases, including NASH (62). The present time-course study revealed that the most prominently overexpressed networks in NAFLD pertained to lipid metabolism, inflammation, apoptosis, fibrosis and angiogenesis, which highlighted their pivotal roles in NASH pathogenesis. These findings were substantiated by time-course histopathological assessments, which closely mirrored the progressive development of NASH in human patients. Furthermore, these data lend strong support to the 'multiple-hit hypothesis', which proposes that the pathogenesis of NASH and fibrosis involves intricate interplay of multiple pathogenic events acting in concert (64).

Comprehensive analysis of genetic transcription patterns in liver tissue samples holds promise for identifying reliable biomarkers that can indicate the progression from steatosis to NASH as it demonstrates notable specificity and sensitivity to dynamic physiological conditions, making it a valuable avenue for biomarker discovery (65). The present transcriptome analysis revealed significantly elevated expression levels of Serpine1 and MMP9 in the livers of mice with NASH. However, a comprehensive assessment of the diagnostic accuracy of these biomarkers for detection of NASH and severe fibrosis has not been performed, and further research is necessary to fully establish their potential as effective diagnostic tools. The findings of the present study established an association between the expression of Serpine1 and Mmp9 in the liver and the progression of NAFLD. As liver pathology advances to NASH, mRNA expression levels of Serpine1 and Mmp9, as well as a corresponding increase in the protein levels of PAI-1and MMP-9. Additionally, data analysis from patient samples obtained from GEO further supported the feasibility of using Serpine1 and MMP9 as hepatic biomarkers with broader applicability. Moreover, the present study demonstrated the use of serum levels of PAI-1 and MMP-9 as noninvasive biomarkers for identifying NASH-related fibrosis. *In vitro* experiments revealed elevated PAI-1 and MMP-9 expression in cells exposed to steatosis and lipotoxicity. Notably, MMP-9 exhibited changes at lower FFA intervention concentrations, while PAI-1 showed changes at higher concentrations, consistent with the results from animal experiments. The primary objective of the present study was to explore the molecular signature and potential biomarkers associated with NASH progression. While the findings offer valuable insights into the underlying disease mechanisms and identify potential biomarkers, these markers were not reverse-confirmed using cell lines deficient in the PAI-1 and MMP-9 genes. Future studies should employ cell line models deficient in these genes to elucidate their specific contributions to disease mechanisms and validate their potential as therapeutic targets. Consequently, the specific roles and molecular mechanisms of PAI-1 and MMP-9 in steatotic cells remain unclear and further elucidation in future experiments.

The PAI-1 protein belongs to the serpin family of serine proteinase inhibitors and serves a significant role in fibrogenesis. Encoded by the Serpine1 gene, this protein has a profibrotic effect on various organs by inhibiting fibrinolysis through modulation of enzymes such as tissue-type and urokinase-type plasminogen activator (uPA) and MMP (66). Serpine1 has emerged as a potential therapeutic target for interventions aimed at treating fibrotic diseases affecting organs such as the skin, lungs, heart, kidney and liver (67). Previous studies have reported increased levels of PAI-1 in the plasma and hepatic tissues of individuals with NAFLD, and this protein has been implicated in various physiological and disease processes, including vascularization, stress response, thrombosis and insulin resistance (68,69). The present study provided evidence which suggested the involvement of Serpine1 in the pathophysiology of NASH-associated fibrosis. While previous omics-based investigations have indicated an association between Serpine1 expression levels in liver tissue from patients with NAFLD and advanced liver fibrosis, the clinical applicability of Serpine1 as a reliable biomarker for NASH diagnosis requires further evaluation (70,71). Within the scope of the present study, a substantial and statistically significant positive association between hepatic expression levels of Serpine1 and the advancement of NAFLD was identified.

Given the intricate pathogenesis of NAFLD involving hepatic cell injury, inflammation and fibrogenesis, biomarkers reflecting the fibrotic pathway often serve as indicators of the disease setting and are cross-sectionally related to NASH (72). PAI-1, which is strongly associated with fibrogenesis, is also associated with ballooning degeneration of hepatocytes and hepatic steatosis. Consequently, serum levels of PAI-1 hold substantial diagnostic potential as a biomarker for severe NASH with fibrosis progression.

There has been growing recognition of the role of MMPs in the degradation of hepatic ECM proteins in models of chronic liver injury (73-75). Among the MMP family, MMP-9 stands out for its implication in the pathogenesis and progression of metastatic human hepatocellular carcinoma (75). Recent studies have highlighted how the remodeling of ECM by MMP-9 contributes to the progression of obesity by regulating adipocyte differentiation (76,77). MMP-9 protein levels have consistently been reported to be elevated in experimental cirrhosis (78,79).

The present study underscores that MMP-9 hepatic mRNA levels could potentially serve as an early diagnostic marker for the prediction of the progression of liver inflammation and injury in individuals with NASH transitioning to liver fibrosis. As anticipated, ELISA substantiates a positive association between serum MMP-9 activity and hepatic levels of MMP-9 protein in HFFD-fed mice. Furthermore, the upregulation of MMP-9 has been associated with an increase in inflammatory biomarkers (80). In summary, these findings suggested that MMP-9 serum levels hold promise as a non-invasive prognostic indicator, particularly for identifying subgroups of NAFL and NASH mice prone to disease deterioration. However, while MMP-9 emerges as a potential biomarker of NAFLD, it is important to recognize that observed changes in MMP-9 levels may not be solely attributable to NAFLD. Numerous factors, including comorbidities (such as pulmonary remodeling, autoimmune diseases, pancreatic cancer, and multiple sclerosis, among others) and individual variations, could influence MMP-9 expression and activity (81). Several mechanisms, such as inflammation, oxidative stress and tissue remodeling processes linked to NAFLD, could also contribute to MMP-9 dysregulation (82). Therefore, further investigations are imperative to ascertain the precise role of MMP-9 in NAFLD development and progression, as well as to identify potential confounding variables affecting its expression levels.

In summary, the present study offered a comprehensive understanding of NAFLD progression and identified potential biomarkers for assessing disease severity from a whole-transcriptome perspective. The results revealed time-dependent regulation of crucial molecules involved in NASH development and fibrous liver disease in HFFD-fed mice. A genetic footprint for NAFLD that signifies active NASH processes and is concurrently detectable with pathological fibrosis was delineated. Hence, the identification of a gene expression pattern discerned in mouse liver could serve as a predictive signature for clinically monitoring patients and developing NASH therapies, with Serpine1 and Mmp9 as the pivotal genes. The proteins, PA-1 and MMP-9, encoded by Serpine1 and Mmp9, respectively, can be quantified in serum samples, offering potential noninvasive diagnostic markers for NASH-related fibrosis progression (83). These findings hold clinical implications and pave the way for further exploration into identifying circulating markers as potential blood-based indicators for detecting hepatic fibrosis. Despite the promising results obtained in the present study, it is important to note that the small sample size of three mice/group may limit the generalizability of the findings and should be considered when interpreting the results. Moreover, prior to incorporating these biomarkers into clinical practice, further studies are imperative to confirm their efficacy and reliability. Assessment of serum levels of PAI-1 and MMP-9 in a larger cohort of patients diagnosed with NAFLD to validate the potential of these two markers as non-invasive biomarkers is required.

Acknowledgements

Not applicable.

Funding

The present study was funded by The National Natural Science Foundation of China (grant nos. 81560688 and 81860745) and Xinjiang Key Laboratory of Natural Active Components and Drug Release Technology (grant no. XJDX1713).

Availability of data and materials

The datasets generated and/or analyzed during the current study are available in the Genome Sequence Archive in The National Genomics Data Center, China National Center for Bioinformation/Beijing Institute of Genomics, Chinese Academy of Sciences (GSA: CRA012922) repository, https://ngdc.cncb.ac.cn/gsa/browse/CRA012922.

Authors' contributions

YZ and JH conceptualized the study. YZ and CM performed the experiments. YZ wrote the original draft preparation; JY and YZ designed the experiments and analyzed data. BW and MY designed and performed the experiments and analyzed data. YZ, JY and JH wrote, reviewed and edited the manuscript; BW performed study visualization; JY supervised the study; JH performed project administration; and JH acquired the funding. YZ and JH confirm the authenticity of all the raw data. All authors have read and approved the final version of the manuscript.

Ethics approval and consent to participate

The experimental protocol was approved by The Xinjiang Animal Testing Center Research Animal Ethics Committee (Urumqi, China; approval no. XJIMM-20210417), and all research involving animals strictly adhered to internationally recognized standards and regulations.

Patient consent for publication

Not applicable.

Competing interests

The authors declare that they have no competing interests.

References

1. Sheka AC, Adeyi O, Thompson J, Hameed B, Crawford PA and Ikramuddin S: Nonalcoholic steatohepatitis: A review. JAMA 323: 1175-1183, 2020.
2. Llovet JM, Willoughby CE, Singal AG, Greten TF, Heikenwälder M, El-Serag HB, Finn RS and Friedman SL: Nonalcoholic steatohepatitis-related hepatocellular carcinoma: Pathogenesis and treatment. Nat Rev Gastroenterol Hepatol 20: 487-503, 2023.
3. Younossi ZM, Koenig AB, Abdelatif D, Fazel Y, Henry L and Wymer M: Global epidemiology of nonalcoholic fatty liver disease-meta-analytic assessment of prevalence, incidence, and outcomes. Hepatology 64: 73-84, 2016.
4. Younossi Z, Anstee QM, Marietti M, Hardy T, Henry L, Eslam M, George J and Bugianesi E: Global burden of NAFLD and NASH: Trends, predictions, risk factors and prevention. Nat Rev Gastroenterol Hepatol 15: 11-20, 2018.
5. Ye Q, Zou B, Yeo YH, Li J, Huang DQ, Wu Y, Yang H, Liu C, Kam LY, Tan XXE, *et al*: Global prevalence, incidence, and outcomes of non-obese or lean non-alcoholic fatty liver disease: A systematic review and meta-analysis. Lancet Gastroenterol Hepatol 5: 739-752, 2020.
6. Farrell GC and Larter CZ: Nonalcoholic fatty liver disease: From steatosis to cirrhosis. Hepatology 43 (2 Suppl 1): S99-S112, 2006.
7. Younossi ZM: Non-alcoholic fatty liver disease-A global public health perspective. J Hepatol 70: 531-544, 2019.

8. Angulo P, Keach JC, Batts KP and Lindor KD: Independent predictors of liver fibrosis in patients with nonalcoholic steatohepatitis. Hepatology 30: 1356-1362, 1999.
9. Tarantino G, Crocetto F, Di Vito C, Creta M, Martino R, Pandolfo SD, Pesce S, Napolitano L, Capone D and Imbimbo C: Association of NAFLD and insulin resistance with non metastatic bladder cancer patients: A cross-sectional retrospective study. J Clin Med 10: 346, 2021.
10. Cotter TG and Rinella M: Nonalcoholic fatty liver disease 2020: The state of the disease. Gastroenterology 158: 1851-1864, 2020.
11. Le MH, Le DM, Baez TC, Wu Y, Ito T, Lee EY, Lee K, Stave CD, Henry L, Barnett SD, *et al*: Global incidence of non-alcoholic fatty liver disease: A systematic review and meta-analysis of 63 studies and 1,201,807 persons. J Hepatol 79: 287-295, 2023.
12. Bedossa P, Poitou C, Veyrie N, Bouillot JL, Basdevant A, Paradis V, Tordjman J and Clement K: Histopathological algorithm and scoring system for evaluation of liver lesions in morbidly obese patients. Hepatology 56: 1751-1759, 2012.
13. Kleiner DE, Brunt EM, Van Natta M, Behling C, Contos MJ, Cummings OW, Ferrell LD, Liu YC, Torbenson MS, Unalp-Arida A, *et al*: Design and validation of a histological scoring system for nonalcoholic fatty liver disease. Hepatology 41: 1313-1321, 2005.
14. Taylor RS, Taylor RJ, Bayliss S, Hagström H, Nasr P, Schattenberg JM, Ishigami M, Toyoda H, Wai-Sun Wong V, Peleg N, *et al*: Association between fibrosis stage and outcomes of patients with nonalcoholic fatty liver disease: A systematic review and meta-analysis. Gastroenterology 158: 1611-1625.e12, 2020.
15. Makri E, Goulas A and Polyzos SA: Epidemiology, pathogenesis, diagnosis and emerging treatment of nonalcoholic fatty liver disease. Arch Med Res 52: 25-37, 2021.
16. Anstee QM, Reeves HL, Kotsiliti E, Govaere O and Heikenwalder M: From NASH to HCC: Current concepts and future challenges. Nat Rev Gastroenterol Hepatol 16: 411-428, 2019.
17. Haas JT, Vonghia L, Mogilenko DA, Verrijken A, Molendi-Coste O, Fleury S, Deprince A, Nikitin A, Woitrain E, Ducrocq-Geoffroy L, *et al*: Transcriptional network analysis implicates altered hepatic immune function in NASH development and resolution. Nat Metab 1: 604-614, 2019.
18. Bedossa P: Diagnosis of non-alcoholic fatty liver disease/non-alcoholic steatohepatitis: Why liver biopsy is essential. Liver Int 38 (Suppl 1): S64-S66, 2018.
19. Ratziu V, Charlotte F, Heurtier A, Gombert S, Giral P, Bruckert E, Grimaldi A, Capron F and Poynard T; LIDO Study Group: Sampling variability of liver biopsy in nonalcoholic fatty liver disease. Gastroenterology 128: 1898-1906, 2005.
20. Park CC, Nguyen P, Hernandez C, Bettencourt R, Ramirez K, Fortney L, Hooker J, Sy E, Savides MT, Alquiraish MH, *et al*: Magnetic resonance elastography vs transient elastography in detection of fibrosis and noninvasive measurement of steatosis in patients with biopsy-proven nonalcoholic fatty liver disease. Gastroenterology 152: 598-607.e2, 2017.
21. Angulo P, Kleiner DE, Dam-Larsen S, Adams LA, Bjornsson ES, Charatcharoenwitthaya P, Mills PR, Keach JC, Lafferty HD, Stahler A, *et al*: Liver fibrosis, but no other histologic features, is associated with long-term outcomes of patients with nonalcoholic fatty liver disease. Gastroenterology 149: 389-397.e10, 2015.
22. Karlsen TH, Sheron N, Zelber-Sagi S, Carrieri P, Dusheiko G, Bugianesi E, Pryke R, Hutchinson SJ, Sangro B, Martin NK, *et al*: The EASL-lancet liver commission: Protecting the next generation of Europeans against liver disease complications and premature mortality. Lancet 399: 61-116, 2022.
23. Angulo P, Hui JM, Marchesini G, Bugianesi E, George J, Farrell GC, Enders F, Saksena S, Burt AD, Bida JP, *et al*: The NAFLD fibrosis score: A noninvasive system that identifies liver fibrosis in patients with NAFLD. Hepatology 45: 846-854, 2007.
24. Graupera I, Thiele M, Serra-Burriel M, Caballeria L, Roulot D, Wong GL, Fabrellas N, Guha IN, Arslanow A, Expósito C, *et al*: Low accuracy of FIB-4 and NAFLD fibrosis scores for screening for liver fibrosis in the population. Clin Gastroenterol Hepatol 20: 2567-2576.e6, 2022.
25. Kjaergaard M, Lindvig KP, Thorhauge KH, Andersen P, Hansen JK, Kastrup N, Jensen JM, Hansen CD, Johansen S, Israelsen M, *et al*: Using the ELF test, FIB-4 and NAFLD fibrosis score to screen the population for liver disease. J Hepatol 79: 277-286, 2023.
26. Day JW and Rosenberg WM: The enhanced liver fibrosis (ELF) test in diagnosis and management of liver fibrosis. Br J Hosp Med (Lond) 79: 694-699, 2018.
27. Bolarin DM and Azinge EC: Biochemical markers, extracellular components in liver fibrosis and cirrhosis. Nig Q J Hosp Med 17: 42-52, 2007.
28. Boyle M, Tiniakos D, Schattenberg JM, Ratziu V, Bugianessi E, Petta S, Oliveira CP, Govaere O, Younes R, McPherson S, *et al*: Performance of the PRO-C3 collagen neo-epitope biomarker in non-alcoholic fatty liver disease. JHEP Rep 1: 188-198, 2019.
29. Wong VW, Adams LA, de Lédinghen V, Wong GL and Sookoian S: Noninvasive biomarkers in NAFLD and NASH-current progress and future promise. Nat Rev Gastroenterol Hepatol 15: 461-478, 2018.
30. Daniels SJ, Leeming DJ, Eslam M, Hashem AM, Nielsen MJ, Krag A, Karsdal MA, Grove JI, Neil Guha I, Kawaguchi T, *et al*: ADAPT: An algorithm incorporating PRO-C3 accurately identifies patients with NAFLD and advanced fibrosis. Hepatology 69: 1075-1086, 2019.
31. Harrison SA, Ratziu V, Boursier J, Francque S, Bedossa P, Majd Z, Cordonnier G, Sudrik FB, Darteil R, Liebe R, *et al*: A blood-based biomarker panel (NIS4) for non-invasive diagnosis of non-alcoholic steatohepatitis and liver fibrosis: A prospective derivation and global validation study. Lancet Gastroenterol Hepatol 5: 970-985, 2020.
32. Matteoni CA, Younossi ZM, Gramlich T, Boparai N, Liu YC and McCullough AJ: Nonalcoholic fatty liver disease: A spectrum of clinical and pathological severity. Gastroenterology 116: 1413-1419, 1999.
33. Tatler AL: Recent advances in the non-invasive assessment of fibrosis using biomarkers. Curr Opin Pharmacol 49: 110-115, 2019.
34. Piazzolla VA and Mangia A: Noninvasive diagnosis of NAFLD and NASH. Cells 9: 1005, 2020.
35. Govaere O, Cockell S, Tiniakos D, Queen R, Younes R, Vacca M, Alexander L, Ravaioli F, Palmer J, Petta S, *et al*: Transcriptomic profiling across the nonalcoholic fatty liver disease spectrum reveals gene signatures for steatohepatitis and fibrosis. Sci Transl Med 12: eaba4448, 2020.
36. Castera L, Friedrich-Rust M and Loomba R: Noninvasive assessment of liver disease in patients with nonalcoholic fatty liver disease. Gastroenterology 156: 1264-1281.e4, 2019.
37. Vilar-Gomez E and Chalasani N: Non-invasive assessment of non-alcoholic fatty liver disease: Clinical prediction rules and blood-based biomarkers. J Hepatol 68: 305-315, 2018.
38. Hoang SA, Oseini A, Feaver RE, Cole BK, Asgharpour A, Vincent R, Siddiqui M, Lawson MJ, Day NC, Taylor JM, *et al*: Gene expression predicts histological severity and reveals distinct molecular profiles of nonalcoholic fatty liver disease. Sci Rep 9: 12541, 2019.
39. Suppli MP, Rigbolt KTG, Veidal SS, Heebøll S, Eriksen PL, Demant M, Bagger JI, Nielsen JC, Oró D, Thrane SW, *et al*: Hepatic transcriptome signatures in patients with varying degrees of nonalcoholic fatty liver disease compared with healthy normal-weight individuals. Am J Physiol Gastrointest Liver Physiol 316: G462-G472, 2019.
40. Loomba R and Sanyal AJ: The global NAFLD epidemic. Nat Rev Gastroenterol Hepatol 10: 686-690, 2013.
41. European Association for the Study of Liver: EASL clinical practical guidelines: Management of alcoholic liver disease. J Hepatol 57: 399-420, 2012.
42. Negi CK, Babica P, Bajard L, Bienertova-Vasku J and Tarantino G: Insights into the molecular targets and emerging pharmacotherapeutic interventions for nonalcoholic fatty liver disease. Metabolism 126: 154925, 2022.
43. Abozaid YJ, Ayada I, van Kleef LA, Vallerga CL, Pan Q, Brouwer WP, Ikram MA, Van Meurs J, de Knegt RJ and Ghanbari M: Plasma proteomic signature of fatty liver disease: The rotterdam study. Hepatology 78: 284-294, 2023.
44. Ratziu V, Francque S and Sanyal A: Breakthroughs in therapies for NASH and remaining challenges. J Hepatol 76: 1263-1278, 2022.
45. Ramanan SP, Mohamed MWF, Aung SS, Sange I and Hamid P: Treatment of fatty liver disease: The present and the future. Cureus 13: e12713, 2021.
46. Fu Y, Zhou Y, Shen L, Li X, Zhang H, Cui Y, Zhang K, Li W, Chen WD, Zhao S, *et al*: Diagnostic and therapeutic strategies for non-alcoholic fatty liver disease. Front Pharmacol 13: 973366, 2022.
47. Hosseini-Esfahani F, Bahadoran Z, Mirmiran P, Hosseinpour-Niazi S, Hosseinpanah F and Azizi F: Dietary fructose and risk of metabolic syndrome in adults: Tehran lipid and glucose study. Nutr Metab (Lond) 8: 50, 2011.
48. Heikkinen S, Argmann CA, Champy MF and Auwerx J: Evaluation of glucose homeostasis. Curr Protoc Mol Biol Chapter 29: Unit 29B.3, 2007.

49. Love MI, Huber W and Anders S: Moderated estimation of fold change and dispersion for RNA-seq data with DESeq2. Genome Biol 15: 550, 2014.
50. Yu G, Wang LG, Han Y and He QY: clusterProfiler: an R package for comparing biological themes among gene clusters. OMICS 16: 284-287, 2012.
51. Livak KJ and Schmittgen TD: Analysis of relative gene expression data using real-time quantitative PCR and the 2(-Delta Delta C(T)) method. Methods 25: 402-408, 2001.
52. McPherson S, Hardy T, Henderson E, Burt AD, Day CP and Anstee QM: Evidence of NAFLD progression from steatosis to fibrosing-steatohepatitis using paired biopsies: Implications for prognosis and clinical management. J Hepatol 62: 1148-1155, 2015.
53. Huang DQ, Terrault NA, Tacke F, Gluud LL, Arrese M, Bugianesi E and Loomba R: Global epidemiology of cirrhosis-aetiology, trends and predictions. Nat Rev Gastroenterol Hepatol 20: 388-398, 2023.
54. Tarantino G, Balsano C, Santini SJ, Brienza G, Clemente I, Cosimini B and Sinatti G: It is high time physicians thought of natural products for alleviating NAFLD. Is there sufficient evidence to use them? Int J Mol Sci 22: 13424, 2021.
55. Santhekadur PK, Kumar DP and Sanyal AJ: Preclinical models of non-alcoholic fatty liver disease. J Hepatol 68: 230-237, 2018.
56. Eng JM and Estall JL: Diet-induced models of non-alcoholic fatty liver disease: Food for thought on sugar, fat, and cholesterol. Cells 10: 1805, 2021.
57. Rinella ME and Green RM: The methionine-choline deficient dietary model of steatohepatitis does not exhibit insulin resistance. J Hepatol 40: 47-51, 2004.
58. Lau JKC, Zhang X and Yu J: Animal models of non-alcoholic fatty liver disease: Current perspectives and recent advances. J Pathol 241: 36-44, 2017.
59. Zhong F, Zhou X, Xu J and Gao L: Rodent models of nonalcoholic fatty liver disease. Digestion 101: 522-535, 2020.
60. Lee JS, Jun DW, Kim EK, Jeon HJ, Nam HH and Saeed WK: Histologic and metabolic derangement in high-fat, high-fructose, and combination diet animal models. ScientificWorldJournal 2015: 306326, 2015.
61. Chen Z, Tian R, She Z, Cai J and Li H: Role of oxidative stress in the pathogenesis of nonalcoholic fatty liver disease. Free Radic Biol Med 152: 116-141, 2020.
62. Sveinbjornsson G, Ulfarsson MO, Thorolfsdottir RB, Jonsson BA, Einarsson E, Gunnlaugsson G, Rognvaldsson S, Arnar DO, Baldvinsson M, Bjarnason RG, *et al*: Multiomics study of nonalcoholic fatty liver disease. Nat Genet 54: 1652-1663, 2022.
63. Tincopa MA and Loomba R: Non-invasive diagnosis and monitoring of non-alcoholic fatty liver disease and non-alcoholic steatohepatitis. Lancet Gastroenterol Hepatol 8: 660-670, 2023.
64. Buzzetti E, Pinzani M and Tsochatzis EA: The multiple-hit pathogenesis of non-alcoholic fatty liver disease (NAFLD). Metabolism 65: 1038-1048, 2016.
65. Naik A, Košir R and Rozman D: Genomic aspects of NAFLD pathogenesis. Genomics 102: 84-95, 2013.
66. Van De Craen B, Declerck PJ and Gils A: The biochemistry, physiology and pathological roles of PAI-1 and the requirements for PAI-1 inhibition in vivo. Thromb Res 130: 576-585, 2012.
67. Ghosh AK and Vaughan DE: PAI-1 in tissue fibrosis. J Cell Physiol 227: 493-507, 2012.
68. Fuchs A, Samovski D, Smith GI, Cifarelli V, Farabi SS, Yoshino J, Pietka T, Chang SW, Ghosh S, Myckatyn TM and Klein S: Associations among adipose tissue immunology, inflammation, exosomes and insulin sensitivity in people with obesity and nonalcoholic fatty liver disease. Gastroenterology 161: 968-981.e12, 2021.
69. Verrijken A, Francque S, Mertens I, Prawitt J, Caron S, Hubens G, Van Marck E, Staels B, Michielsen P and Van Gaal L: Prothrombotic factors in histologically proven nonalcoholic fatty liver disease and nonalcoholic steatohepatitis. Hepatology 59: 121-129, 2014.
70. Wang S, Li Y, Liu N, Shen W, Xu W and Yao P: Identification of glucose metabolism-related genes in the progression from nonalcoholic fatty liver disease to hepatocellular carcinoma. Genet Res (Camb) 2022: 8566342, 2022.
71. Meng Q, Li X and Xiong X: Identification of Hub genes associated with non-alcoholic steatohepatitis using integrated bioinformatics analysis. Front Genet 13: 872518, 2022.
72. Peiseler M, Schwabe R, Hampe J, Kubes P, Heikenwälder M and Tacke F: Immune mechanisms linking metabolic injury to inflammation and fibrosis in fatty liver disease-novel insights into cellular communication circuits. J Hepatol 77: 1136-1160, 2022.
73. Mittal R, Patel AP, Debs LH, Nguyen D, Patel K, Grati M, Mittal J, Yan D, Chapagain P and Liu XZ: Intricate functions of matrix metalloproteinases in physiological and pathological conditions. J Cell Physiol 231: 2599-2621, 2016.
74. Hemmann S, Graf J, Roderfeld M and Roeb E: Expression of MMPs and TIMPs in liver fibrosis-a systematic review with special emphasis on anti-fibrotic strategies. J Hepatol 46: 955-975, 2007.
75. Thieringer FR, Maass T, Anthon B, Meyer E, Schirmacher P, Longerich T, Galle PR, Kanzler S and Teufel A: Liver-specific overexpression of matrix metalloproteinase 9 (MMP-9) in transgenic mice accelerates development of hepatocellular carcinoma. Mol Carcinog 51: 439-448, 2012.
76. Wagner J, Kumar Y, Lautenbach A, von Kroge P, Wolter S, Mann O, Izbicki J, Gagliani N and Duprée A: Fatty acid-binding protein-4 (FABP4) and matrix metalloproteinase-9 (MMP9) as predictive values for nonalcoholic steatohepatitis (NASH). Lipids Health Dis 22: 1, 2023.
77. Goyale A, Jain A, Smith C, Papatheodoridi M, Misas MG, Roccarina D, Prat LI, Mikhailidis DP, Nair D and Tsochatzis E: Assessment of non-alcoholic fatty liver disease (NAFLD) severity with novel serum-based markers: A pilot study. PLoS One 16: e0260313, 2021.
78. Kossakowska AE, Edwards DR, Lee SS, Urbanski LS, Stabbler AL, Zhang CL, Phillips BW, Zhang Y and Urbanski SJ: Altered balance between matrix metalloproteinases and their inhibitors in experimental biliary fibrosis. Am J Pathol 153: 1895-1902, 1998.
79. Kim JW, Lee SH, Jeong SH, Kim H, Ahn KS, Cho JY, Yoon YS and Han HS: Increased urinary lipocalin-2 reflects matrix metalloproteinase-9 activity in chronic hepatitis C with hepatic fibrosis. Tohoku J Exp Med 222: 319-327, 2010.
80. Bruschi F, D'Amato C, Piaggi S, Bianchi C, Castagna B, Paolicchi A and Pinto B: Matrix metalloproteinase (MMP)-9: A realiable marker for inflammation in early human trichinellosis. Vet Parasitol 231: 132-136, 2016.
81. Vandooren J, Van den Steen PE and Opdenakker G: Biochemistry and molecular biology of gelatinase B or matrix metalloproteinase-9 (MMP-9): The next decade. Crit Rev Biochem Mol Biol 48: 222-272, 2013.
82. Kim KE, Lee J, Shin HJ, Jeong EA, Jang HM, Ahn YJ, An HS, Lee JY, Shin MC, Kim SK, *et al*: Lipocalin-2 activates hepatic stellate cells and promotes nonalcoholic steatohepatitis in high-fat diet-fed Ob/Ob mice. Hepatology 77: 888-901, 2023.
83. Indira Chandran V, Wernberg CW, Lauridsen MM, Skytthe MK, Bendixen SM, Larsen FT, Hansen CD, Grønkjær LL, Siersbæk MS, Caterino TD, *et al*: Circulating TREM2 as a noninvasive diagnostic biomarker for NASH in patients with elevated liver stiffness. Hepatology 77: 558-572, 2023.

Copyright © 2023 Zhao et al. This work is licensed under a Creative Commons Attribution-NonCommercial-NoDerivatives 4.0 International (CC BY-NC-ND 4.0) License.